Scaling photogrammetry: A comparative evaluation and metrological assessment across small- and meso-scale domains

Precision Engineering 92 (2025) 124–140

Contents lists available at ScienceDirect

Precision Engineering

journal homepage: www.elsevier.com/locate/precision

Scaling photogrammetry: A comparative evaluation and metrological assessment across small- and meso-scale domains

Mattia Trombini [a], Giacomo Maculotti [a], Domenico Augusto Maisano [a], Alfonso Pagani [b], Fiorenzo Franceschini [a,*]

[a] Department of Management and Production Engineering (DIGEP), 10129, Torino, Italy
[b] Department of Mechanical and Aerospace Engineering (DIMEAS) Politecnico di Torino, 10129, Torino, Italy

ARTICLE INFO

Handling Editor: Dr. Masonori Kunieda

Keywords:
Photogrammetry
Multiscale analysis
Performance benchmark
Measurement uncertainty
Design of experiment
Camera calibration
Laser scanner

ABSTRACT

Photogrammetry inspection is a Machine Vision (MV) technique intensely employed to assess the geometry of industrial assets across several measurement scales, ranging from micro-scales focusing on surface to meso- and large-scales targeting geometrical features and shape.

This research endeavors to conduct a comprehensive comparative evaluation of photogrammetry across different dimensional scale domains, aiming to establish a framework for assessing performance levels in various aspects, driven by the portability of the instrumentation, measurement performance and proficiency. Central to the current methodology is employing a single camera, driven by the research's forward-looking goal to integrate drone technology equipped with a solitary camera as the primary payload. In addition, this work presents a statistical quantitative investigation where the most relevant sources of uncertainty are taken into account. Three case studies about a small truss, a ball-bar, and a collaborative robot accompany the analysis.

Finally, this study proposes a framework for assessing the expanded uncertainty and the relative uncertainty across the scales, revealing that the latter decreases with larger measurand, providing a value of 0.2 % when dealing with meso-scale objects.

Acronyms

3D	Three-dimensional
ANOVA	Analysis of Variance
C2C	Cloud-to-cloud
DoE	Design of Experiment
DoF	Degree of Freedom
DPU	Data Processing Unit
FCCS	Local camera coordinate system
FWCS	World coordinate reference system
FDM	Fused Deposition Modeling
GUM	Guide to the Expression of Uncertainty in Measurement
IQR	Interquartile range
LSDM	Large-Scale Dimension Metrology
LVM	Large-Volume Metrology
MInd4Lab	Manufacturing Industry 4.0 Laboratory
MPE	Maximum Permissible Error
MV	Machine Vision
MVS	Machine Vision System
NDT	Non-destructive testing
PEEK	Polyether Ether Ketone
PUMA	Procedure for Uncertainty MAnagement
RANSAC	RANdom SAmple Consensus
RGB	Red-green-blue
UAV	Unmanned aerial vehicle
VIM	International Vocabulary of Metrology

(*continued on next column*)

(*continued*)

1. Introduction

The progression of structural inspection techniques within the aviation [1] and maritime [2] industries has primarily been guided by the objectives of increasing precision, enhancing efficiency, and bolstering safety. Traditional approaches have included hands-on visual inspections [3], ultrasonic pulse techniques [4,5], and X-ray imaging [6,7], all of which have been fundamental in paving the way for contemporary inspection methods. While effective, visual inspection is

* Corresponding author. Quality Engineering and Management Group, Department of Management and Production Engineering, Politecnico di Torino, Corso Duca degli Abruzzi 24, 10129, Torino, Italy.
E-mail address: fiorenzo.franceschini@polito.it (F. Franceschini).

https://doi.org/10.1016/j.precisioneng.2024.12.002
Received 5 March 2024; Received in revised form 2 November 2024; Accepted 1 December 2024
Available online 3 December 2024

inherently subjective and constrained by the accessibility of the structure under examination. The limitations in timing, interpretability, and accessibility arise from its static nature, reliance on subjective assessments, and dependency on an unobstructed view [8]. These challenges have spurred the adoption of noncontact methods, notably various non-destructive testing (NDT) techniques [9,10] to perform reliable inspection on structures. These techniques enable detailed analysis without necessitating physical contact with the structure. Amongst the others NDT, Machine Vision Systems (MVSs) are extremely attractive since they couple high flexibility with high informativeness [11] and can exploit diverse technologies, e.g., single cameras [12], multiple-camera [13,14] systems, line lasers coupled with cameras [15], while often leveraging on machine learning for feature extraction and identification [12] and multi-sensor data fusion [16,17].

Photogrammetric inspection, a subset of MVS, represents an advanced non-contact geometrical characterization method. It employs cameras to assess the surface condition of industrial assets. The methodology and its associated algorithms are advancing, and the scope of research interest in its application for NDT is expanding [18]. This progression is attributable to photogrammetry's advantages, such as cost-effectiveness, rapid execution, and the elimination of physical contact requirements [19]. In contrast to traditional NDT sensors that measure discrete points, photogrammetry offers the capability to conduct full-field measurements. Photogrammetry produces an informative and accurate overview but the speed of reconstruction can be slow and lacks the ability to reveal internal structural details. Furthermore, photogrammetry allows for more frequent measurements, which can reduce the workload and health risks for inspectors [20,21], particularly in the context of Large-Scale Dimension Metrology (LSDM) [16,22–24]. The emergence of camera and computer vision-based sensors has marked a significant advancement in the field, offering promising tools for the non-contact, remote measurement of structural responses [25,26]. Photogrammetry allows the measurement with high accuracy and precision of small [27,28] and large geometric features [22,29,30], while coupling the capability of simply managing free-form shaped parts [31].

The process of photogrammetry generates an output known as a point cloud [32]. A three-dimensional (3D) point cloud consists of three-dimensional points defined by their X, Y, and Z coordinates within a spatial reference frame, each representing a part of an object's surface [33,34]. Additional attributes like red-green-blue (RGB) color values and surface normals can be associated with each point, depending on the capturing sensor [34]. Furthermore, 3D point clouds are inherently unstructured and lack a specific order, contrasting with 2D images represented on a regular grid [32]. The quality of photogrammetric reconstruction depends heavily on the image overlap and coverage within the process [35].

A relevant aspect discussed in the literature delves into the integration of photogrammetry with unmanned aerial vehicles (UAVs). Ioli et al. [36] presented a UAV photogrammetry-based procedure for accurately evaluating cracks in concrete bridges, underscoring the potential of UAVs combined with photogrammetry in bridge inspections and damage assessments. Zhao et al.'s research [26] introduced a dam emergency monitoring and inspection model using UAV-based photogrammetry, showcasing notable enhancements in monitoring and inspection efficiency. Furthermore, concerning large-scale structures, Benzon et al. [37] proposed a framework for classifying paint defects and damage via coupling images collected from a drone and/or several LiDAR scans.

Within this wide range of scenarios, photogrammetry is challenged by application in high precision manufacturing for both micro- [28], meso- [31] and large-scale dimensions [29]. These pose strict requirements on the manufacturing tolerances to be met and verified by the inspection system, which for the LSDM can go significantly beyond the typical $0.1/\sqrt{x}$ ratio of the tolerance to nominal dimension (x) [29]. A comprehensive study of the impact of different factors on the optimum point cloud is presented in Ref. [38], while measuring, modeling, and correcting systematic errors in 3D coordinate measurement are discussed in Ref. [39]. However, a structured investigation of photogrammetric metrological performance across multiple scales is missing in the literature, to the best of the author's knowledge. The current work aims to contribute with a qualitative and quantitative discussion of the relevance of some influence factors on different measurement scales and by providing measurement uncertainty estimations extending beyond the systematic errors. This study aims to provide a comparative evaluation of photogrammetry's capabilities across various scales of interest, establishing a set of performance levels used to categorize aspects such as simplicity/time of use, the measurement process, data analysis, and scale-dependent proficiency. Furthermore, a significant portion of this work is devoted to an in-depth assessment of expanded uncertainty. The employed statistical methodology entails a robust estimation of uncertainty at larger scales, where conducting experimental plans specifically designed to study uncertainty propagation is not feasible. Moreover, for the purposes of this study, a single camera was employed due to the intention of advancing the research through the application of a drone outfitted with one camera as its primary payload towards robust and traceable applications of quantitative visual inspection through UAV for LSDM, e.g., in aerospace and nautical field.

The paper is organized as follows: the fundamentals of photogrammetry are introduced in Section 2, Section 3 describes the experimental setup and the methodology; then, the results are shown in Section 4 and the conclusions are drawn in Section 5.

2. Fundamentals of photogrammetry

Photogrammetry employs a distributed array of strategically positioned cameras within a designated measurement volume. This technique aims to accurately distinct visual features within each camera's field of view, as depicted in Fig. 1. In this study, a single camera is employed, and the camera network is intended to be represented by frames captured from multiple positions. Typically, an external Data Processing Unit (DPU) is responsible for processing the captured data, establishing connectivity either wirelessly or via a cable system. In this context, the three-dimensional coordinates of a specific optical marker, denoted as M_j, are correlated with the two-dimensional coordinates of the corresponding image point, $P_{i,j}$, on the projection plane of the i-th camera. This correlation incorporates the camera's technical specifications, positioning, and orientation (see Fig. 2).

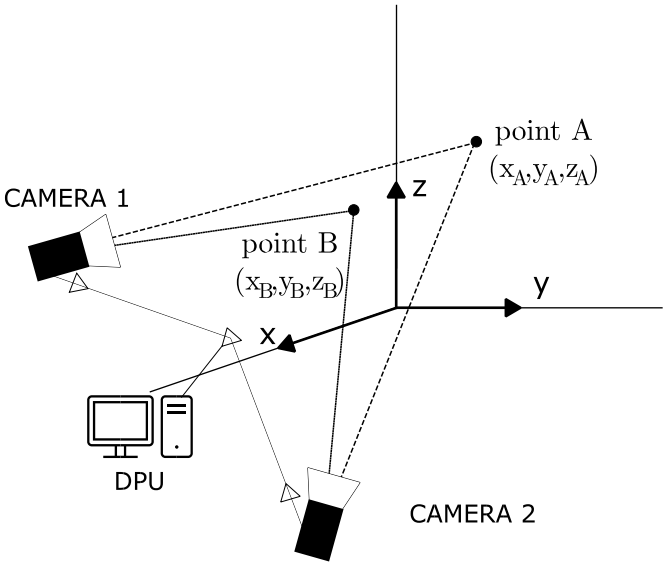

Fig. 1. Illustration of camera network setup in a photogrammetric system, utilizing DPU Bluetooth connectivity.

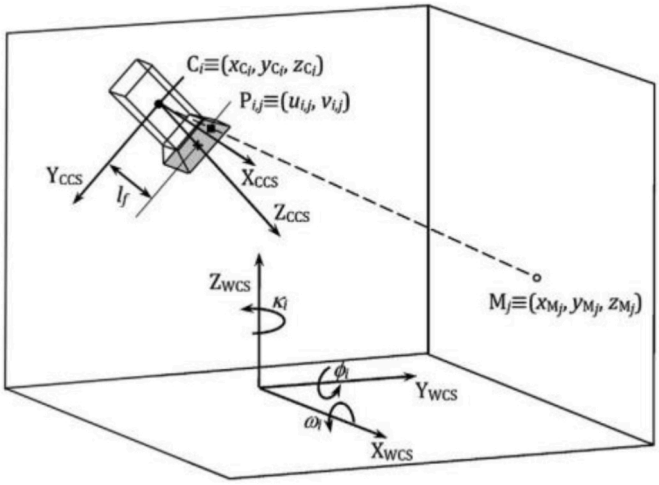

Fig. 2. Setup of a generic camera-based localization problem in 3D space (adapted from Ref. [23]).

The process is executed through the application of collinearity equations using homogeneous coordinates [40,41]:

$$\lambda_i \times \begin{bmatrix} u_{i,j} \\ v_{i,j} \\ 1 \end{bmatrix} = \boldsymbol{K}_i \times \boldsymbol{W}_i \times \begin{bmatrix} x_{M_j} \\ y_{M_j} \\ z_{M_j} \\ 1 \end{bmatrix} = \boldsymbol{P}_i \times \begin{bmatrix} x_{M_j} \\ y_{M_j} \\ z_{M_j} \\ 1 \end{bmatrix} \tag{1}$$

where λ_i is the non-zero scale factor and $\boldsymbol{K}_i$ is the 3x4 matrix of internal parameters, defined as follows:

$$\boldsymbol{K}_i = \begin{bmatrix} u_{f_i} & 0 & u_{0_i} & 0 \\ 0 & v_{f_i} & v_{0_i} & 0 \\ 0 & 0 & 1 & 0 \end{bmatrix} \tag{2}$$

where u_{0_i} and v_{0_i} represent the coordinates of the image center, while u_{f_i} and v_{f_i} correspond to the focal length components related to the camera. The matrix $\boldsymbol{W}_i$ is a 4x4 representation of external parameters, and expressed as:

$$\boldsymbol{W}_i = \begin{bmatrix} & \boldsymbol{R}_i & & -x'_{C_i} \\ & & & -y'_{C_i} \\ & & & -z'_{C_i} \\ 0 & 0 & 0 & 1 \end{bmatrix} \tag{3}$$

where $\boldsymbol{R}_i$ is the rotation matrix that establishes the relationship between the world coordinate reference system (F_{WCS}) and the local camera coordinate system (F_{CCS}), whereas x'_{C_i}, y'_{C_i} and z'_{C_i} are the coordinates of the projection center C_i in the local camera coordinate system F_{CCS}. $\boldsymbol{R}_i$ is defined as follows:

$$\boldsymbol{R}_i = \begin{bmatrix} \cos(\kappa_i)\cos(\phi_i) & \cos(\kappa_i)\sin(\phi_i)\sin(\omega_i) - \sin(\kappa_i)\cos(\omega_i) & \cos(\kappa_i)\sin(\phi_i)\cos(\omega_i) + \sin(\kappa_i)\sin(\omega_i) \\ \sin(\kappa_i)\cos(\phi_i) & \sin(\kappa_i)\sin(\phi_i)\sin(\omega_i) + \cos(\kappa_i)\cos(\omega_i) & \sin(\kappa_i)\sin(\phi_i)\cos(\omega_i) - \cos(\kappa_i)\sin(\omega_i) \\ -\sin(\phi_i) & \cos(\phi_i)\sin(\omega_i) & \cos(\phi_i)\cos(\omega_i) \end{bmatrix} \tag{4}$$

where κ_i, ϕ_i and ω_i are the orientation angles for the i-th camera. $\boldsymbol{P}_i = \boldsymbol{K}_i \times \boldsymbol{W}_i$ is commonly known as camera projection matrix.

In order to minimize lens distortion errors, appropriate corrections are applied to the image coordinates. The predominant types of imaging errors, namely radial, tangential, and skewness distortions, are addressed [40,41]. Consequently, the collinearity equation is adapted by incorporating distortion coefficients, which are introduced as follows:

$$\lambda_i \times \begin{bmatrix} \widetilde{u}_{i,j} \\ \widetilde{v}_{i,j} \\ 1 \end{bmatrix} = \lambda_i \times \begin{bmatrix} 1 & 0 & \delta u_{R_{i,j}} + \delta u_{T_{i,j}} + \delta u_{S_{i,j}} \\ 0 & 1 & \delta v_{R_{i,j}} + \delta v_{T_{i,j}} \\ 0 & 0 & 1 \end{bmatrix} \begin{bmatrix} u_{i,j} \\ v_{i,j} \\ 1 \end{bmatrix} = \boldsymbol{P}_i \times \begin{bmatrix} x_{M_j} \\ y_{M_j} \\ z_{M_j} \\ 1 \end{bmatrix} \tag{5}$$

where $\delta u_{R_{i,j}}$ and $\delta v_{R_{i,j}}$ account for the radial distortion, $\delta u_{T_{i,j}}$ and $\delta v_{T_{i,j}}$ represent the tangential distortion and, eventually, $\delta u_{S_{i,j}}$ is the skeweness-related term. The distortion coefficients are expressed as polynomial functions, as outlined in Eq. (6):

$$\begin{cases} \delta u_{R_{i,j}} = f_1\left(u_{i,j}, v_{i,j}, k_{C1_i}, k_{C2_i}, k_{C5_i}\right) \\ \delta v_{R_{i,j}} = f_2\left(u_{i,j}, v_{i,j}, k_{C1_i}, k_{C2_i}, k_{C5_i}\right) \\ \delta u_{T_{i,j}} = f_3\left(u_{i,j}, v_{i,j}, k_{C3_i}, k_{C4_i}\right) \\ \delta v_{T_{i,j}} = f_4\left(u_{i,j}, v_{i,j}, k_{C3_i}, k_{C4_i}\right) \\ \delta u_{S_{i,j}} = f_5\left(v_{i,j}, \alpha_i\right) \end{cases} \tag{6}$$

with k_{C1_i}, k_{C2_i}, k_{C3_i}, k_{C4_i}, k_{C5_i} and α_i known as correction parameters. k_{C1_i}, k_{C2_i} and k_{C5_i} are involved in the radial distortion definition, k_{C3_i} and k_{C4_i} account for the tangential distortion, and α_i is used for the skewness distortion. Additional details on the polynomial formulation of these coefficients are provided in Ref. [30].

In the context of photogrammetry, localization is the process of deducing the three-dimensional coordinates of a marker, denoted as M_j, from its two-dimensional projections in images from several cameras. As delineated in Eqs. (1) and (3), a single camera's view limits the determination to only the direction of M_j. To fully ascertain M_j's coordinates, observations from a minimum of two camera positions are necessary. This method involves the intersection of multiple directional vectors. A common practice is to use three points of overlap: the minimum two for accuracy and an additional one for redundancy.

The calibration of the network is a critical step that involves estimating the 16 specific parameters for each camera, as listed in Table 1. The internal parameters represent the camera technical features, the correction parameters are related to the distortions, and the external parameters pertain to the position and orientation of each camera with respect to a reference frame. An in-depth exploration of the methods for extracting these parameters and their role in enhancing photogrammetric accuracy is discussed in Ref. [30]. Proper parameters calibration is essential to ensure precise and reliable photogrammetric data. In measurement and mapping processes, accurate scaling is imperative and is achieved by determining known distances between at least three measured points. The scaling procedure can be accomplished by

Table 1
Summary of internal, correction and external parameters to be set up during calibration.

Internal parameters	Correction parameters	External parameters
u_{0_i}	k_{C1_i}	x_{C_i}
v_{0_i}	k_{C2_i}	y_{C_i}
u_{f_i}	k_{C3_i}	z_{C_i}
v_{f_i}	k_{C4_i}	κ_i
	k_{C5_i}	ϕ_i
	α_i	ω_i

calibrating the measurement system parameters, employing reference artifacts with known dimensions, or utilizing coded markers whose positions and relative distances are precisely known. Coded markers can be used with the aim of multiple capturing simultaneously under a single viewing angle, and geometric relations determine the distance and pose of the end. Coded markers offer a highly distinguishable design with strong visual characteristics and, in most cases, also feature specific coding as a safeguard against misidentification [42].

3. Instrumentation and methods

3.1. Instrumentation

The experimental setup incorporates a Basler acA2500-14uc camera [43], selected for its suitable resolution capabilities. The key specifications of this camera include a resolution of 2590 x 1942 pixels, a sensor format of 1/2.5", pixel size measuring 2.2 × 2.2 μm, and a frame rate of 14 fps. Complementing the camera, a Basler Lens C125-0818-5M − P [44] is used, featuring a focal length of 8.11 mm with a tolerance of ±5 %, an optimum working distance of 0.5 m, and an optimum magnification of 0.016. The selected camera and objective represent a customer-grade and cost-effective industrial camera solution, with limited performances for scales lower than 1 mm. Additionally, the camera system interfaces with a DPU having the following specifications: an Intel Core i7-1195G7 processor (2.90 GHz, 4 cores), 16 GB DDR4 RAM, Intel Iris Xe Graphics, and running on Windows 11. A rotary table reduces camera movement and maintains the required resolution. This table, measuring approximately 400 × 400 mm^2, facilitates controlled rotation, as illustrated in Fig. 3.

The table enables the rotation of the object under measurement while maintaining the camera in a stationary position. Notably, the setup allows for rotation angle control, ensuring accurate (with a resolution of 1°) positioning for each image capture.

The point cloud generated as an output in this study is produced using Agisoft Metashape© [45], a standalone software designed for image-based 3D modelling. Agisoft Metashape© aims to create professional-quality 3D content from still images, such as point clouds or textured meshes. It is based on the latest multi-view 3D reconstruction technology and operates with arbitrary images, proving efficient in controlled and uncontrolled conditions. A significant advantage of this software is the complete automation of image alignment and 3D model reconstruction processes.

Fig. 3. Rotary table employed for the photogrammetric process located within the Manufacturing Industry 4.0 Laboratory (MInd4Lab) at the Politecnico di Torino.

3.2. Reference artifacts

In the context of this research endeavor, a thorough investigation is presently being conducted, focusing on the meticulous analysis of three distinct object types distinguished by their diverse dimensions. These objects are deliberately considered significant artifacts for the purpose of this study.

- A truss structure fabricated through the Fused Deposition Modeling (FDM) [46] process with a length of 170 mm and a thickness of 3 mm. The truss is manufactured with an APIUM P220 printer out of Polyether Ether Ketone (PEEK) [47], and Fig. 4 illustrates the in-plane representation of the artefact.
- A ball-bar, defined as a steel rod with two spheres, each featuring a nominal radius of 19 mm, threaded onto its opposing ends (see Fig. 5). The specified nominal distance between the centers of the two spheres is established at 100 mm.
- A collaborative robot (cobot) UR3e (see Fig. 6), equipped with a gripper end-effector [48], located within the Manufacturing Industry 4.0 Laboratory (MInd4Lab) at the Politecnico di Torino.

The truss structure, with its geometry of considerable complexity and notably slender segments, presents an intriguing case for this study. This object is readily manufacturable and amenable to investigation when positioned on top of the rotary table. The ball-bar has a simpler geometry but can be easily pre-calibrated; RANdom SAmple Consensus (RANSAC) algorithms for sphere fitting are efficiently utilized. The cobot features a larger footprint, broadening the scope of photogrammetric application to diverse scales. Moreover, the cobot underscores certain constraints inherent to photogrammetry, notably through its glossy surfaces, which pose challenges to the accurate reconstruction of the point cloud. Lastly, the application of RANSAC algorithms for plane fitting is straightforward. According to Refs. [29,31], objects with a characteristic length, denoted as L_c, exceeding 1000 mm are commonly classified in the domain of Large-Volume Metrology (LVM), while the mesoscale typically ranges from 0.5 mm to 1000 mm. Since the dimensions under consideration in this paper do not exceed 1000 mm, the following terminology is suggested for the purpose of establishing a precise classification:

- Small-scale: pertaining to objects of diminutive size, characterized by L_c within the range:

$$1\ mm < L_c \leq 100\ mm \tag{7}$$

- Meso-scale: pertaining to objects of medium size, characterized by L_c within the range:

$$100\ mm < L_c \leq 1000\ mm \tag{8}$$

As further elaborated in Section 3.4, the truss and ball-bar reside within the small-scale domain, whereas the collaborative robot is categorized within the meso-scale.

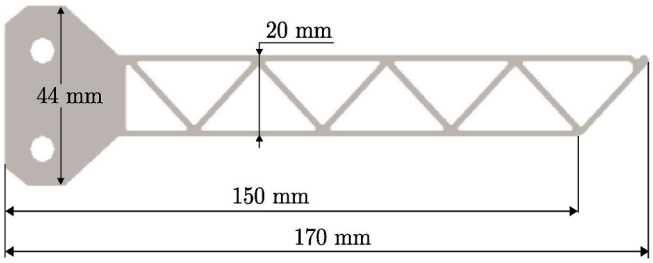

Fig. 4. In-plane representation for the PEEK FDM-printed truss.

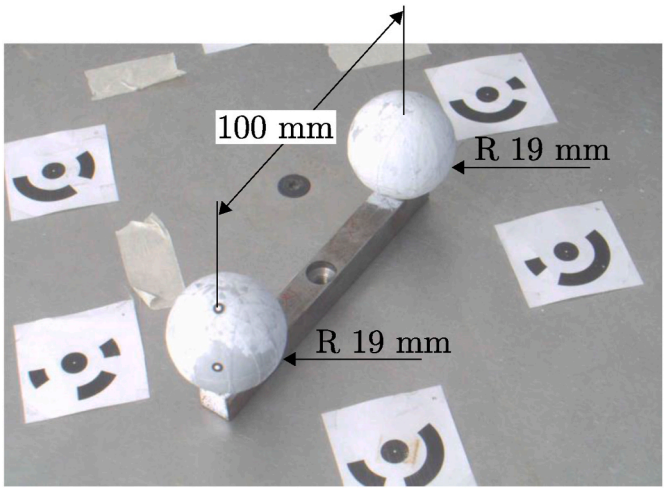

Fig. 5. Image of the ball-bar placed over the rotary table.

3.3. Multiscale qualitative comparison

This research aims to provide a comprehensive exploration of the use of photogrammetric instrumentation in the process of object reconstruction, with a particular focus on its applicability across a spectrum of different scales. To facilitate a systematic comparison between scale domains, a set of sub-criteria is defined and presented in Table 2. A five-level ordinal scale is proposed, categorizing performance levels as: Low (L), Low/Medium (L/M), Medium (M), Medium/High (M/H), and High (H) [49,50]. The hierarchical relationship between these performance levels is represented as follows:

$$L \prec L/M \prec M \prec M/H \prec H \tag{9}$$

Thus, ascending the scale corresponds to an enhancement in performance.

3.4. Quantitative characterization

This study performs a quantitative evaluation of the photogrammetry with respect to measurement scales. First of all, considering literature and best practices, a quantitative investigation of factors widely recognized as liable for affecting reconstruction quality is carried out. Specifically, a Design of Experiment (DoE) [51] is proposed as a crucial component of the statistical analysis to elucidate how the output variables are affected by input factors and their interactions. The application of Analysis of Variance (ANOVA) to the DoE framework enables to separate contributions of output variability attributable to factors under control from other uncontrolled sources and random errors. Such investigation is essential to design the measurement process while aiming at maximizing measurement performances.

Furthermore, the ANOVA analysis provides the percentual contribution to the sum of squares (SS%), calculated as follows:

$$SS\% = \frac{SS_i}{SS_{TOT}} \times 100 \tag{10}$$

where SS_i is the sum of squares related to the i-th factor, and SS_{TOT} is the total sum of squares. Quantitative evaluations are carried out on selected response variables of the three measurands described in Section 3.2. Specifically, for the truss, it is considered the thickness D_{truss} (see Fig. 7), for the ball-bar the radius of the sphere D_{sphere} and the distance between their centers $D_{ballbar}$ (see Fig. 8), and for the cobot the distance between the arm roll and the centerpoint of the gripping end-effector D_{cobot} (see Fig. 9).

D_{truss}, D_{sphere}, $D_{ballbar}$, and D_{cobot} are defined as the response variables of the case studies in this work, and the relative reference values are summarized in Table 3.

Due to the compliant material out of which the truss and the ball bar were made out of, it was unreliable to measure the selected features dimensions with a CMM. The calibration of the truss and ball bar reference artifacts has been carried out by means of a structured light project system ATOS GOM ScanBox Series 4 [53]. The ATOS GOM was calibrated according to ISO 10360–13:2021 [54,55], showing a length measurement error of −0.004 mm on a length of 160 mm (MPE of 34 μm), and spherical size measurement error of 0.0045 mm on a diameter of 25 mm (MPE of 15 μm); the ISO 10360-13 procedure was performed replicating 10 times in 3 different poses the measurements of a CMM-calibrated ball plate artefact (with uncertainty of 1 μm) in an accredited laboratory, providing an overall of 30 measurements. The API iScan 3D laser line scanner [56] (with uncertainty of 14.64 μm

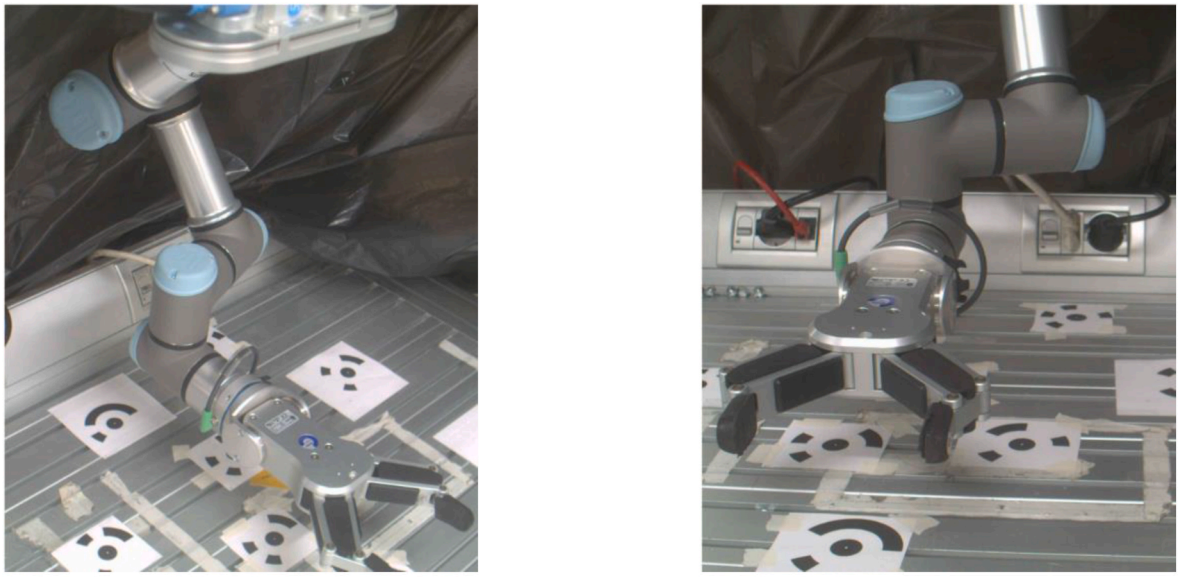

(a) **(b)**

Fig. 6. Collaborative robot UR3e, with relative experimental setup. Information about geometry, dimensions and footprint can be retrieved in Ref. [48].

Table 2
Description of (sub-)criteria used for multiscale qualitative comparison.

Criteria		Description
1. Simplicity/time of use		
1.1 Preparation	1.1.1 Portability	Related to the spatial footprint of the instrumentation
	1.1.2 Accessory tools	Related to the utilization of tools for enhancing the photogrammetric process
	1.1.3 Number of markers	Related to the quantity of coded benchmarks
	1.1.4 Marker placement	Related to the positioning of markers around the component
	1.1.5 Set-up time	Related to the duration for positioning, warming up, initializing the instrument, and attaching any accessories
1.2 Measurement	1.2.1 Operator dexterity	Related to the skill and efficiency of the operator in handling and operating the photogrammetric equipment
	1.2.2 Number of images	Related to the quantity of images required for the photogrammetric process
	1.2.3 Time for acquisition	Related to the total time taken to capture all necessary images for the photogrammetric analysis
1.3 Data analysis	1.3.1 Processing time	Related to the time required to process the captured images into useable data or models
	1.3.2 Post-processing heaviness	Related to the complexity and resource intensity of post-processing tasks, including data cleaning and model refinement
2. Measurement performance		
2.1 Information content		Related to the amount of information extractable from a reconstruction
2.2 Reconstruction quality		Related to the accuracy, resolution, and overall quality of the 3D models or data sets generated from the photogrammetric process
2.3 Statistical investigation		Related to the capability of conducting robust statistical analyses at a given scale
2.4 Noise		Related to the presence of extraneous elements or artifacts in the reconstruction not belonging to the component (environment)
2.5 Detection of small geometrical variation		Related to the identification of minute changes in an object's shape or dimensions that are small in comparison to the overall scale of the object
3. Scale-dependent proficiency		
3.1 Skill improvement		Related to the enhancement of operator skills when operating at different scales
3.2 Effective applicability		Related to the practical convenience of using the photogrammetric tool at that scale, compared to other metrological instruments

Fig. 7. Reconstructed point cloud of the truss with the definition of D_{truss}.

retrieved during the calibration of a spatial length as per ISO 10360–10:2021 [57] on a ball plate artefact calibrated by an accredited laboratory with CMM measurements having uncertainty of 1 μm) is employed to calibrate the collaborative robot. By observing the reference value and comparing the value with Eqs. (7) and (8), it is determined that the truss and the ball-bar fall into the small-scale category, while the cobot is classified within the meso-scale. The uncertainty of the geometric features reported in Table 3 is computed at a 95 % confidence level combining different contributions, as per PUMA method [58,59]. The propagated contributions are: the uncertainty of the CMM measurements performed in the accredited laboratories; the accuracy reported in the calibration certificates of the measuring instruments (as reported above according to ISO 10360) and as the MPE for the truss (for calibration on the ball plate did not include any feature on such a small scale); the reproducibility estimated as a type A contribution as the standard deviation of five replicated measurements of the relevant geometrical features when performing measurements changing the position of the artefact on the support plate and changing the number of acquisitions; the fitting error due to RANSAC, estimated as standard deviation of 100 replications; the contribution of micro-geometric errors. The latter were estimated as the planarity error for the truss (as a type A contribution from a CMM measurement), and as MPE for the other measurands. As far as the accuracy is concerned, although more refined approaches have been proposed [60], the methodology here relies on the average error estimated from replicated measurements of a calibrated artefact reported in the calibration certificate obtained as per ISO 10360-10 (for the Laser Scanner) and as per ISO 10360-13 (for the GOM ScanBox) [54,55,57,61,62]. Fig. 10 details the traceability chain from accredited laboratory CMMs to Optical 3D CMS and Laser Scanner

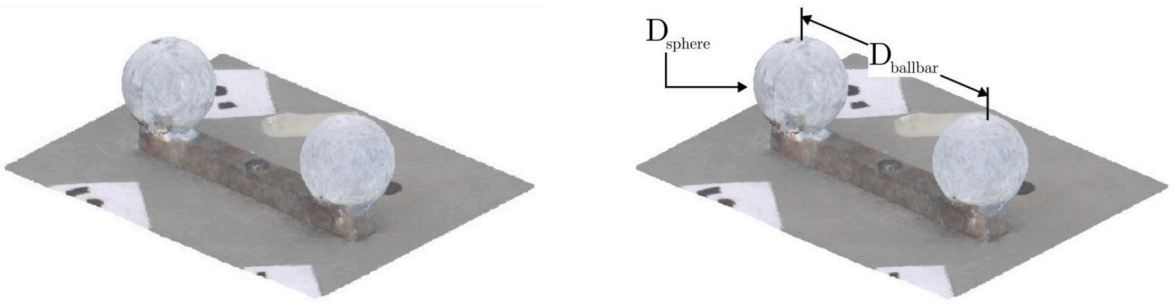

Fig. 8. Reconstructed point cloud of the ball-bar (a), and definition of the radius D_{sphere} and $D_{ballbar}$ (b).

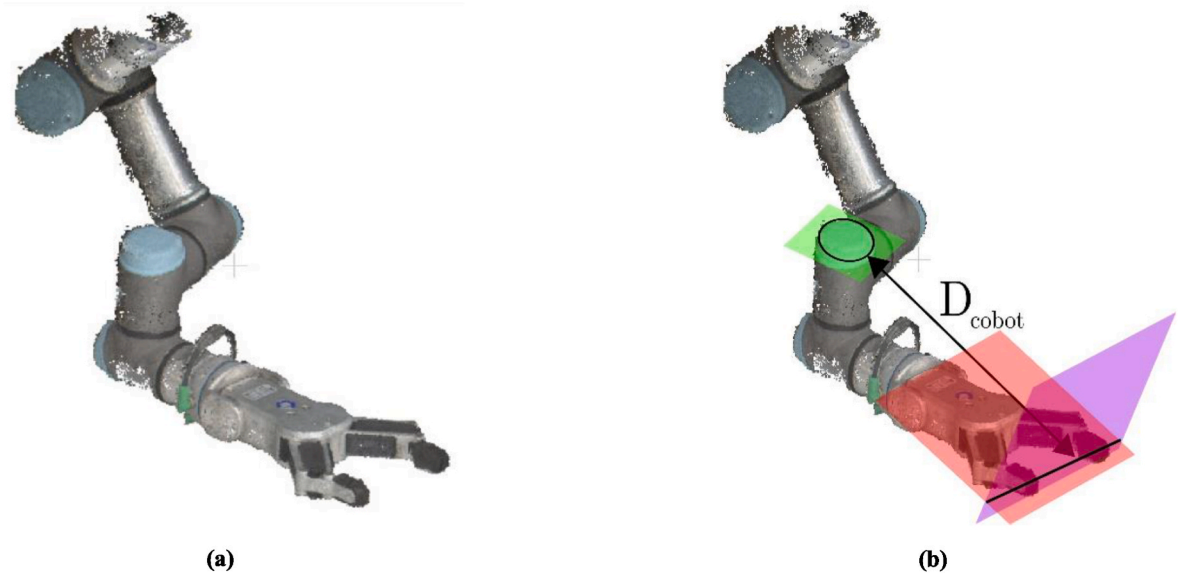

Fig. 9. Reconstructed point cloud of the cobot (a), and definition of the distance D_{cobot} (b).

Table 3
Calibrated reference values for the relevant geometrical features and measurement uncertainty. Notice the decreasing relative uncertainty for increasing measurement scale. The term k_{REF} is the "coverage factor" [52].

L_c	Reference value/mm	k_{REF}	U_{REF}/μm	U%/-	Metrological tool
Dtruss	3.13	2.04	55.7	1.79 %	ATOS GOM ScanBox Series 4 [53]
Dsphere	18.87	2.31	42.3	0.22 %	ATOS GOM ScanBox Series 4 [53]
Dballbar	99.33	2.36	39.7	0.04 %	ATOS GOM ScanBox Series 4 [53]
Dcobot	363.95	2.23	84.6	0.02 %	API iScan 3D laser line scanner [56]

to, finally, photogrammetry.

3.4.1. Factor number of images

The factor number of images is chosen by means of a preliminary investigation on its impact on the coverage of the artefact, i.e., the truss. Specifically, three distinct configurations are analyzed.

- Employment of 72 images taken at every 5° interval of rotation on the rotating table; namely Setup 1.
- Employment of 36 images taken at every 10° interval of rotation on the rotating table; namely Setup 2.
- Employment of 24 images taken at every 15° interval of rotation on the rotating table; namely Setup 3.

The investigation into the influence of coverage is undertaken through a comparative analysis between the photogrammetric cloud and a reference geometry, as illustrated in Fig. 11. The reference geometry is acquired using the ATOS GOM ScanBox Series 4 system [53]. This comparative assessment is conducted quantitatively, assessing cloud density and the cloud-to-cloud (C2C) euclidean distance between the photogrammetric output and the reference data. This approach promotes the determination of the minimum number of images essential for achieving a good-quality reconstruction of the artifacts, thus establishing the minimum level for the factor number of images. As further discussed in Section 4.2, Setup 3 is ruled out from the DoE analysis since the dispersion of C2C distances is too large compared to Setups 1 and 2 [38].

3.4.2. Sources of uncertainty

The identification of factors inducing systematic errors in the measurements allows distinguishing different contributions to the measurement uncertainty towards a metrological characterization of the system. In this work, different contributions to measurement uncertainty are considered, namely reproducibility, bias, resolution, uncertainty of the reference, and numerical sources due to measurement algorithms [63,64]. The first term considered is the reproducibility, denoted as u^2_{REPR}. According to the International Vocabulary of Metrology (VIM) [65], reproducibility is the closeness of agreement between the results of measurements of the same measurand under changed conditions. These conditions may include variations in the measurement method, observer, instrument, reference standard, location, conditions of use, and time. Reproducibility is quantitatively expressed in terms of the dispersion characteristics of the results. Accordingly, it will be evaluated as the total variance from the ANOVA analysis [66]. This choice, although liable for including contributions from systematic sources of variability, is conservative and allows generalization of the estimation for cases in which the control of the factors is not possible, e.g., whenever multiple camera poses are required to obtain a sufficient coverage and reconstruction quality.

Measurements taken in a point cloud involve point-to-point, point-to-line, point-to-plane, line-to-line, line-to-plane, and plane-to-plane distances. Consequently, the RANSAC-based technique [67] is extensively employed to construct the best-fitting primitive for a specific subset of the point cloud, identifying two sources of uncertainty.

- A systematic contribution, as the deviation of the inliers with respect to the fitting primitive, denoted as $u^2_{RANS,S}$.
- A random contribution, represented by the variance of the measured value derived from multiple applications of RANSAC to the same dataset, is indicated as $u^2_{RANS,R}$..

Another significant contribution is the bias, referring to the closeness of agreement between the output and the true or accepted reference value. It measures the systematic error in a measurement process and is expressed as:

$$e = \left|\overline{L_c} - L_{c,REF}\right| \tag{11}$$

Assuming the bias has a uniform distribution, its contribution to variance is quantified as:

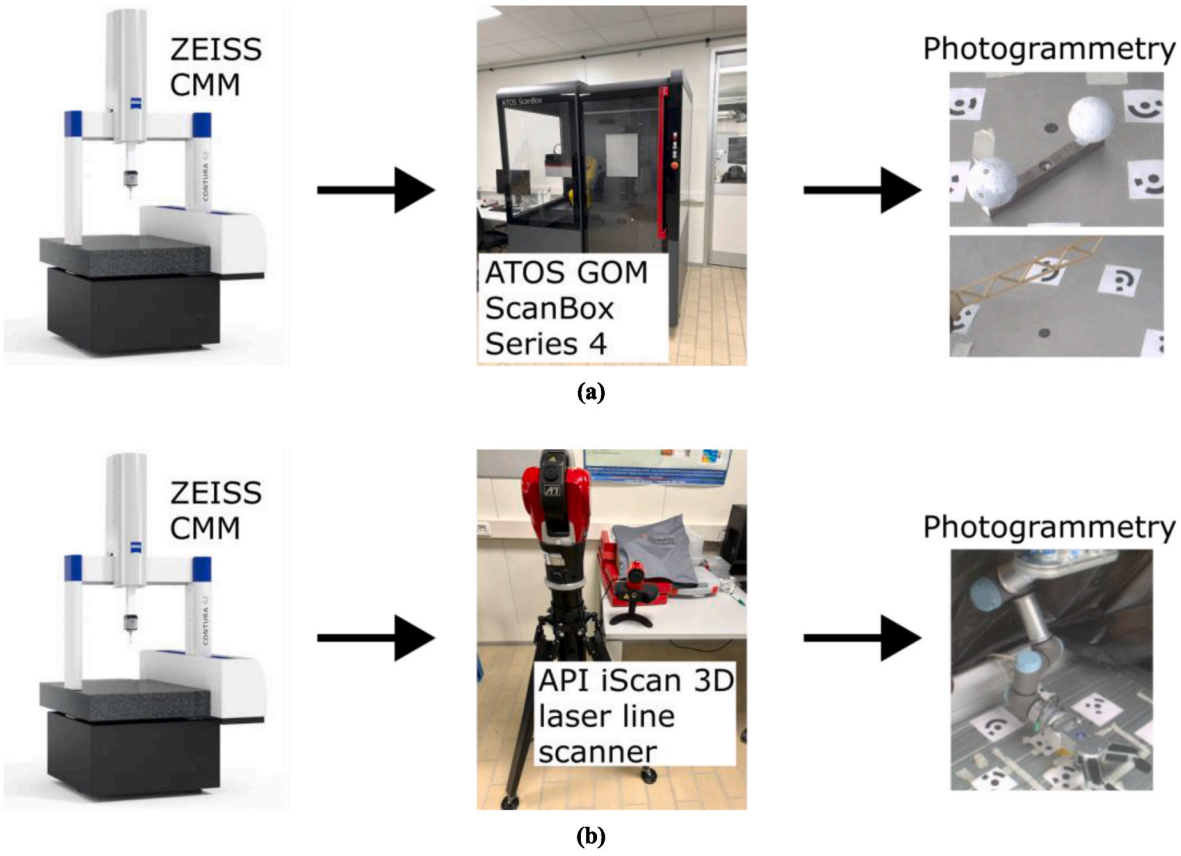

Fig. 10. Traceability chain from accredited laboratory CMM to (a) Optical 3D CMS and (b) Laser Scanner to, finally, photogrammetry.

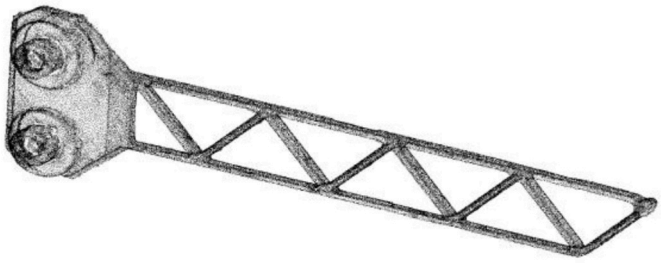

Fig. 11. Point cloud of the truss reconstructed with structured light project system ATOS GOM ScanBox Series 4 [53].

$$u_{BIAS}^2 = \frac{e^2}{3} \tag{12}$$

The variance composition must also consider the uncertainty of the reference measurement:

$$u_{REF}^2 = \left(\frac{U_{REF}}{k_{REF}}\right)^2 \tag{13}$$

Finally, another contribution is from the resolution of the photogrammetry, defined as the smallest change in a quantity being measured that causes a perceptible change in the corresponding indication:

$$u_{RES}^2 = \frac{(RES/2)^2}{3} \tag{14}$$

The composition of the variance then considered the sum of each contribution:

$$u^2 = u_{REPR}^2 + u_{RANS,S}^2 + u_{RANS,R}^2 + u_{BIAS}^2 + u_{REF}^2 + u_{RES}^2 \tag{15}$$

Hence, the standard uncertainty can be easily extracted:

$$u = \sqrt{(u^2)} \tag{16}$$

Nevertheless, a coverage broader than the standard uncertainty is needed, including the concept of *expanded uncertainty* denoted as U [52]. This is expressed as:

$$U = k \cdot u \tag{17}$$

The calculation of the effective Degrees of Freedom (DoFs) ν_y utilizes the Welch-Satterthwaite equation, presented as follows:

$$\nu_y = \left\lfloor \frac{u^4}{\sum_{j=1}^{n} \frac{u_j^4}{\nu_j}} \right\rfloor \tag{18}$$

In determining the expanded uncertainty, the coverage factor is selected to correspond with a 95 % confidence interval. Finally, the uncertainty evaluation takes into account the percentage relative uncertainty, defined as follows:

$$U\% = \frac{U}{\overline{L_c}} \times 100 \tag{19}$$

where $\overline{L_c}$ is the average characteristic length for the considered measurements based on the entire dataset gathered from the DoE.

4. Preliminary results

The current section presents and discusses the results concerning the reconstruction of the photogrammetric output of the case studies presented in Section 3.2. In particular, the investigation focuses on the analysis of the image coverage on the point cloud and continues with the

discussion concerning the qualitative comparison across different scales; finally, a statistical investigation is carried out. To begin with, the reconstructed clouds are presented, and the geometrical features used for the analysis are briefly shown for the truss in Fig. 7, for the ball-bar in Fig. 8 and for the cobot in Fig. 9.

4.1. Issues in glossy surface reconstruction

In the context of photogrammetric reconstruction (sub-criterion 1.3.2 of Table 2), it is essential to acknowledge potential challenges that can impact the quality of the point cloud. These factors affect the "Measurement performances" (criterion 2 of Table 2), in terms of information content (2.1), the capability of providing a robust evaluation for quantitative investigation (2.3) and of detecting relatively small features (2.5) and is liable of increasing measurement noise (2.4). Specifically, certain materials, such as metallic and glossy components, pose unique difficulties in achieving accurate and precise reconstructions. The challenges associated with the point cloud representation of shiny surfaces have been the subject of considerable research and practical experimentation. Various methodologies have been explored and implemented to mitigate issues with glossy surfaces, e.g., the application of matte spray. The quality of the reconstruction, in terms of geometrical correspondence to the real object, can be influenced by low-contrast images [68], reflectance [69], and black components [70]. In this work, each sphere of the ball-bar is treated with a matte spray (see Fig. 5) to significantly reduce their reflectiveness and generate a good spherical reconstruction, as discernible in Fig. 8. In photogrammetry, challenges arise with inconsistent feature detection on glossy surfaces and a lack of visible texture on objects, leading to potential inaccuracies in 3D reconstructions due to difficulties in matching and tracking surface details across images.

Focusing on the UR3e collaborative robot [48], Fig. 12 delineates a significant area for reconstructing the point cloud, notably emphasizing the glossy region enclosed within the red dashed box. The reconstructed cloud is discernible in Fig. 13, with a magnification on the glossy area. Finally, Fig. 14 contains the C2C distance of the cloud from a reference cloud, generated by using the API iScan 3D laser line scanner [56].

By observing the reconstruction, some considerations can be drawn.

- By observing Fig. 13, the shape of the metallic part is significantly affected by the issues with the glossy surface, as the cylindricity is wholly misplaced.
- The quantification of the C2C distance between the photogrammetric cloud and the reference clearly shows significant discrepancies in the metallic section, where the distance is around 9 mm on average, as pointed out in Fig. 14.

4.2. Number of images

In this section, the investigation focuses on the effect of image coverage on the point cloud of the truss, as introduced in Section 3.4.1.

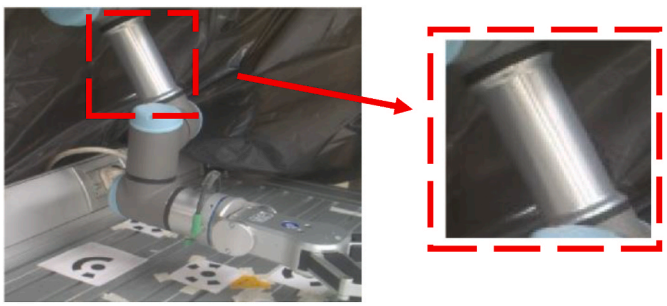

Fig. 12. Image of the collaborative robot UR3e [48], with a magnification in the glossy metallic section.

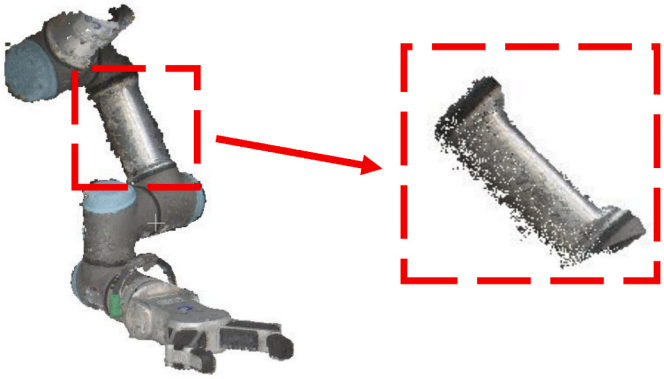

Fig. 13. Point cloud of the collaborative robot UR3e [48], with a magnification in the glossy metallic section.

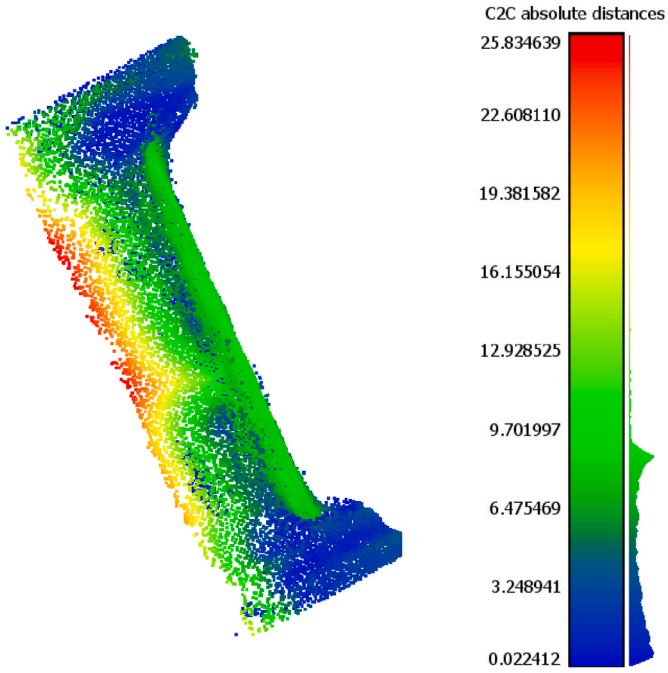

Fig. 14. C2C distance in mm between the photogrammetric point cloud and the reference cloud, obtained by employing the API iScan 3D laser line scanner [56].

The histogram depicting the C2C distance between the photogrammetric point cloud and the reference cloud is displayed in Fig. 15. Remarkably, the distribution of distances conforms to a right-skewed pattern. Consequently, the chosen statistical parameters for the comparison among the three cases encompass the median and the interquartile range (IQR). In conjunction with the point count within the clouds, a comprehensive comparative analysis of these parameters is elaborated in Table 4.

By analyzing the results, some comments can be raised.

- Significant disparities are not observed in the histograms between Setup 1 and Setup 2 (refer to Fig. 15a and b), a finding corroborated by the data presented in Table 4. Specifically, it is worth noting that the median value, when using 36 images, exhibits a modest increase of 2.4 % when compared to the output generated from 72 images, while the IQR registers a 1.1 % increment. In stark contrast, Setup 3 yields substantially higher results, a trend evident from the pronounced right-skewness displayed in Fig. 15c. By employing

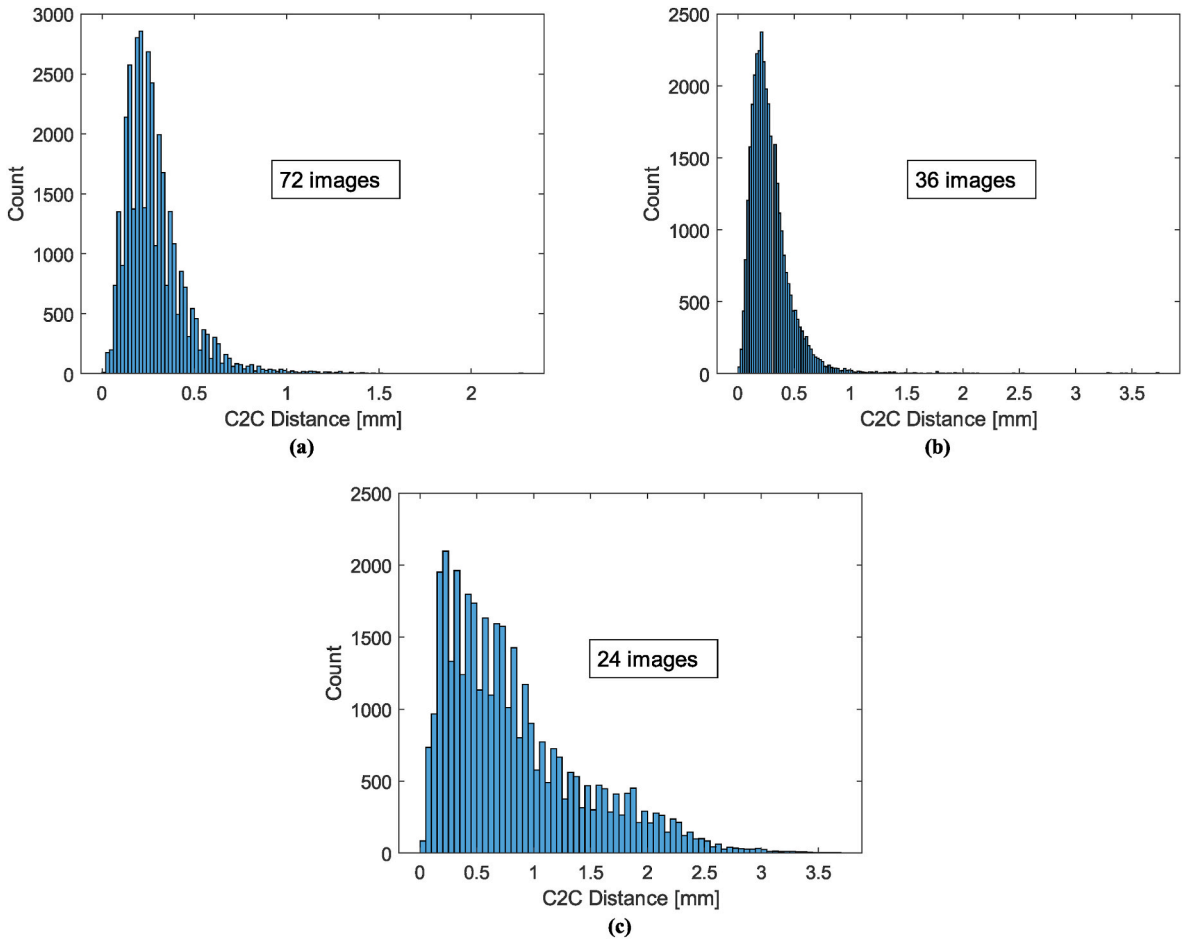

Fig. 15. Histograms of C2C distance between the reference cloud and photogrammetric cloud reconstructed with (a) 72 images, (b) 36 images, and (c) 24 images.

Table 4
Comparison of point cloud density, median C2C and IQR C2C between the photogrammetric cloud and the reference.

Number of images	Number of points	Median C2C/mm	IQR C2C/mm
72	60503	0.253	0.180
36	57704	0.259	0.182
24	57435	0.671	0.785

nonparametric Mood's Median Test [71], the statistical significance of the difference in the medians is highlighted at a confidence interval of 95 %.

- The inclusion of a higher number of images as input results in a denser point cloud, as confirmed by the data presented in Table 4. Specifically, the density increase is noteworthy when using more images as input. Respectively, Setup 1 and Setup 2 exhibit an increase in density of 5.3 % and 0.5 % compared to Setup 3.
- The significant dispersion of C2C distance in Setup 3 (24 images) justifies the choice of considering the factor number of images on two levels: 36 and 72 images, respectively.

4.3. Results of qualitative comparison

As anticipated, the aim of this study is to compare the photogrammetric capabilities across two distinct scales. The criteria defined, while essential, are inherently subjective; their selection is rooted in the workflow specific to the photogrammetric process. Each criterion is treated as independent, without incorporating any synthesis or aggregation. Fig. 16 illustrates the profile chart for the two scales under

Table 5
Summary of performance levels of the photogrammetric process across the two scales of interest. L Low, L/M Low/Medium, M Medium, M/H Medium/High, H High performance.

Comparison criteria		Performance Level	
		Small-scale	Meso-scale
1. Simplicity/time of use			
1.1 Preparation	1.1.1 Portability	H	H
	1.1.2 Accessory tools	M/H	L
	1.1.3 Number of markers	H	M
	1.1.4 Marker placement	H	L/M
	1.1.5 Set-up time	H	M
1.2 Measurement	1.2.1 Operator dexterity	M/H	M
	1.2.2 Number of images	M/H	L/M
	1.2.3 Time for acquisition	M/H	L/M
1.3 Data analysis	1.3.1 Processing time	M/H	M
	1.3.2 Post-processing heaviness	L/M	M
2. Measurement performance			
2.1 Information content		M	M
2.2 Reconstruction quality		M/H	M
2.3 Statistical investigation		H	L/M
2.4 Noise		L	M
2.5 Detection of small geometrical variation		L/M	M/H
3. Scale-dependent proficiency			
3.1 Skill improvement		M	M/H
3.2 Effective applicability		L/M	M/H

examination. A plot resembling a histogram is presented in Fig. 17a to facilitate a comprehensive understanding of the comparison between the scales. Fig. 17b encapsulates the median performance level among the macro criteria, namely simplicity/time of use, measurement performance, and scale-dependent proficiency. Additionally, a comprehensive summary of the results is provided in Table 5, where each criterion is systematically delineated.

4.3.1. Simplicity/time of use

Portability:	The use of a camera and markers for both small-scale and meso-scale objects offers an advantage in terms of portability. This commonality in equipment reduces the need for specialized tools, making it a convenient choice for various scenarios. Additionally, the compact nature of the equipment makes it easy to transport to different locations, ensuring flexibility in use. Consequently, both scales require compact instrumentation, and no relevant differences can be detected. Furthermore, the footprint of the instrumentation is significantly lower than that of other metrological tools, e.g., laser scanners and laser trackers [53,56]. It is important to note that the ease of transport and setup of photogrammetric equipment significantly enhances its applicability in diverse field conditions.
Accessory tools:	It is convenient to use a calibrated instrument to facilitate the image acquisition process. In detail, the use of a rotary table makes it possible to keep the camera in a fixed position and still acquire images of the component from multiple angles. For this work, a rotary table is used, as shown in Fig. 3. In addition, the use of the table allows the markers to be placed on top of the plate in a fixed manner, thus making it possible to avoid extracting their coordinates. Due to the size of the table, only small-scale transportable objects can be placed on top of the table, while larger objects are more complicated to transport and place. For objects of a significantly larger scale that align with the Large-Volume Metrology domain, the utilization of tools as rotary tables is totally impractical.
Number of markers:	The scale of the object also impacts the number of markers needed. Larger reference scales typically require a greater number of markers to ensure accurate reconstruction. This consideration is essential for planning marker placement and assessing the practicality of marker deployment in different scenarios.
Marker placement:	The ease of marker placement is more apparent with small-scale objects, whose size and accessibility facilitate convenient positioning. Conversely, meso-scale objects present challenges due to spatial limitations and accessibility, potentially increasing setup complexity. Optimization of marker placement for meso-scale objects is key to enhancing efficiency in larger-scale photogrammetric applications. For larger scales, coded markers can potentially be substituted by environmental features, discernible through the application of MVSs, leading to an increase in the performance level of the criterion.
Set-up time:	Setup duration is pivotal in measurement processes. Small-scale objects offer efficiency advantages, requiring minimal surface treatment and camera startup time, thus rapidly becoming operational. Accessory tools further expedite marker placement. In contrast, meso-scale objects necessitate extended setup times due to manual camera positioning and marker coordinate extraction.
Operator dexterity:	The skill level of an operator is crucial in achieving accurate measurements. For small-scale objects, the operator's role is generally straightforward, focusing on framing a significant number of markers in each image. However, when dealing with meso-scale objects, the task becomes more complex. The operator must adeptly capture a sufficient number of markers along with a substantial portion of the object in each frame.
Number of images:	The number of images required for measurement is influenced by the object's scale. Small-scale objects necessitate fewer images to achieve adequate coverage due to their compact size. In contrast, larger objects demand a higher number of images to ensure comprehensive coverage.
Time for acquisition:	The choice of equipment and techniques can significantly impact the time required for data acquisition. The use of a rotary table is particularly advantageous for reducing acquisition time, as it eliminates the need for continuous camera movement. In contrast, meso-scale objects typically require manual camera repositioning, increasing the time needed to acquire a complete dataset of images. This difference in acquisition methods affects the overall efficiency of the measurement process.
Processing time:	Data processing time is directly influenced by the number of images collected during the measurement process. In the case of small-scale objects, where fewer images are required, the data processing time is shorter. This allows for a more aggressive setting of reconstruction quality, resulting in higher-quality reconstructions. However, for meso-scale objects, the larger number of images leads to longer processing times, which may necessitate a trade-off between processing time and reconstruction quality.
Post-processing heaviness:	Post-processing efforts are primarily dedicated to noise reduction. Small-scale objects tend to have more pronounced noise due to their smaller size, making noise reduction a significant aspect of the post-processing workflow.

(continued on next column)

(continued)

4.3.2. Measurement performan

Information content:	Regardless of scale, photogrammetric methods generally provide good geometry reconstruction and color consistency. However, as depicted in Ref. [33], no semantic information is present in the point cloud, and it is necessary to pass through a processing phase. Consequently, no relevant differences arise between the two scales.
Reconstruction quality:	The quality and density of the point cloud are influenced by factors such as the number of images acquired and the specific components encompassed within each frame. It becomes evident that a larger quantity of images results in a more favorable reconstruction quality. Furthermore, as the project's scale increases, the camera's precise positioning becomes imperative for the accurate localization of component features. Consequently, the reconstruction quality increasingly relies upon the camera's spatial orientation, thereby augmenting the complexity of achieving appropriate coverage. Other factors that can affect the point cloud are discussed in Section 4.1.
Statistical investigation:	With small-scales, proceeding with an experimental campaign to fully propagate the measurement uncertainty is less time-consuming. If the scale grows, the number of images required is greater, and the time to perform a robust uncertainty assessment becomes untenable. More details are given in Section 4.4.
Noise:	The proportion of objects captured relative to the surrounding environment differs between small and meso-scales. For meso-scale objects, the environment has less impact on the captured images due to the object's dominance in the frame. In contrast, as the scale decreases, the object occupies a smaller portion of the frame, leading to increased environmental influence.
Detection of small geometrical variation:	When the objective is to detect damage or non-conformities at the micro-scale in an object's geometry, the choice of measurement method becomes critical. Photogrammetry may not be the most suitable option for small-scale objects because the variations in their dimensions are more likely to fall below the measurement instrument's uncertainty threshold. More details can be retrieved in Section 4.4.

4.3.3. Scale-dependent proficiency

Skill improvement:	At smaller scales, the technical and scientific skill enhancement of the operator is less pronounced, as the process tends to be simpler. However, with the increase in scale, the efficiency of the operator's skills can be enhanced, as the selection of exposure settings and the positioning of the camera become critical tasks for reducing processing time.

(continued on next page)

(*continued*)

Effective applicability:	Assessing the suitability of photogrammetry is crucial, especially in relation to the specific context and objectives of the measurement. For small-sized structures, photogrammetry might not always be the most efficient approach, particularly in scenarios where high precision and accuracy are paramount. The level of detail achievable through photogrammetry may not suffice for comprehensive experimental evaluation.

By observing the results, some comments can be raised.

- For the simplicity/time of use criterion at the small-scale, the median is predominantly in the Medium/High range, whereas the meso-scale is in the Medium range. Consequently, in terms of the first macro criterion, i.e., the Simplicity/time of use, the small-scale demonstrates a notably higher performance compared to the meso-scale, as depicted in Fig. 17b.
- Upon examining Fig. 16, the profile charts exhibit multiple intersections regarding the measurement performance, indicating no distinct superiority of one scale over another. On the other hand, scale-dependent proficiency shows the higher performance of the meso-scale, as clearly shown in Fig. 17a and b.

4.4. Statistical investigation

In this section, the results of the statistical quantitative investigation are presented and discussed following the methodology introduced in Section 3.4. Small-scale objects can be placed on the rotary table, allowing for the individual variation of certain factors of interest to conduct a thorough investigation into their effect on reproducibility and systematic errors. The time required for completing a full cycle of photogrammetric reconstruction can be significantly reduced due to the rotation of the table. This notwithstanding, each replication took approximately 30'. Measurements were performed in common room with a combination of artificial and natural light, which, thus, varied through the experiments, resulting in variable illumination conditions. As depicted in Section 4.2, the large dispersion of C2C distances obtained with Setup 3 leads the factor number of images to be set on 2 levels. Specifically, as summarized in Table 6, three factors are considered, including three replications, and following a $2 \times 2 \times 2 \times 3$ DoE.

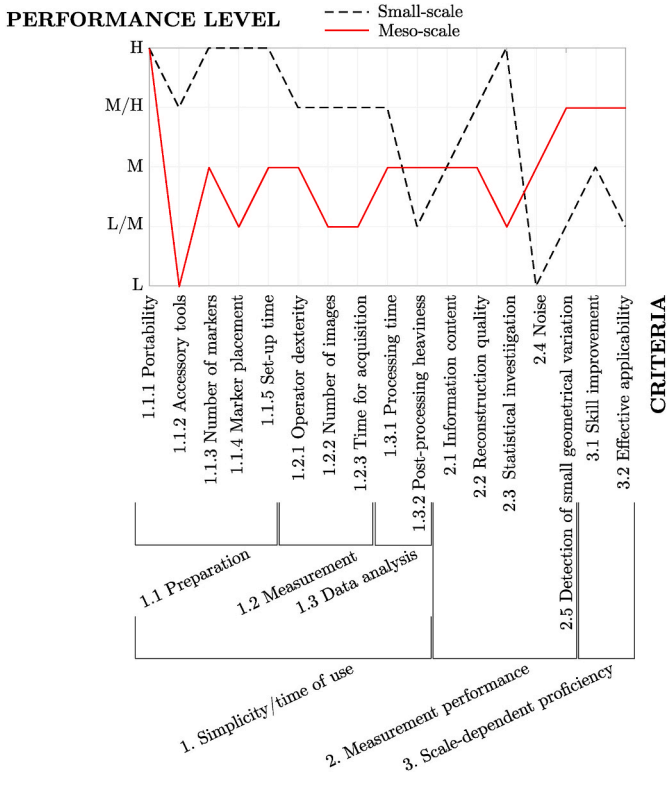

Fig. 16. Chart summarizing the performance levels for the two scales of interest. The performance level related to each criterion is expressed using a five-level ordinal scale: L Low, L/M Low/Medium, M Medium, M/H Medium/High, H High performance.

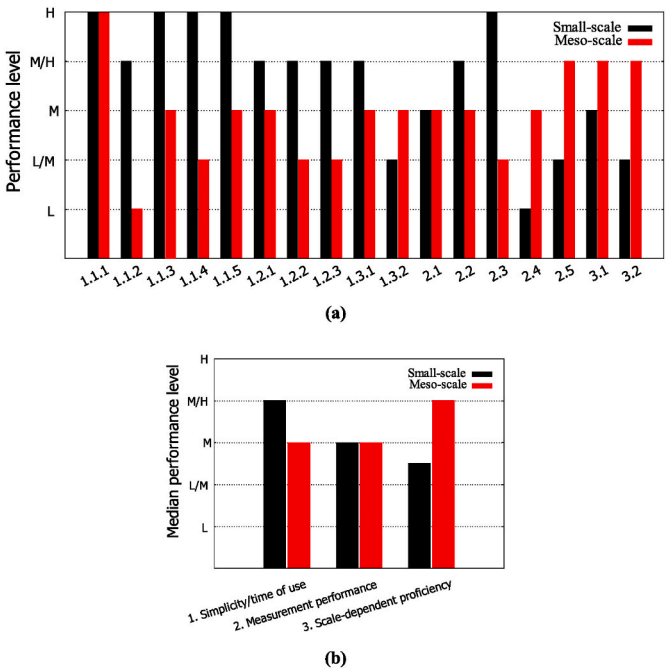

Fig. 17. Histogram of (a) sub-criteria and (b) median performance level of the macro criteria for the two scales. L Low, L/M Low/Medium, M Medium, M/H Medium/High, H High performance. The sub-criteria follow the enlisting provided in Table 2.

Table 6
Influence Factors considered in the Design of Experiments.

Factors	Levels	Description
Camera position	2	More and less tilted with respect to the measurand
Component collocation	2	More and less centered with respect to markers
# of images	2	{36; 72}

The ANOVA table (see Table 7) is utilized to assess the statistical significance of the considered factors, including their interactions. For both the truss thickness and the distance between the centers of the spheres in the ball-bar measurements. The table includes the number of degrees of freedom for each factor, the p-value, and the percentage contribution to the sum of squares (SS%).

By observing Table 7 and it can be concluded that the camera

Table 7
Analysis of Variance for D_{truss} and $D_{ballbar}$ as output.

	D_{truss}			$D_{ballbar}$		
	ν	SS%	p-value	ν	SS%	p-value
Camera position	1	57.86 %	<0.01	1	41.02 %	<0.01
Component collocation	1	0.25 %	0.71	1	12.05 %	0.04
Nr of images	1	1.40 %	0.39	1	3.67 %	0.24
2-Way Interactions	3	9.18 %	0.20	3	2.57 %	0.79
3-Way Interactions	1	2.76 %	0.23	1	1.94 %	0.38
Error	16	28.54 %	0.23	16	38.74 %	0.38

position is the most significant factor. The SS% clearly indicates that the variability is primarily influenced by the camera position and by unexplained random error. However, maintaining a fixed camera position during the inspection of an object is not always possible, especially for large-scale structures. In fact, in the case of the cobot, multiple positions were required to ensure adequate coverage and quality of the reconstruction, thus forcing to disregard such factor in the ANOVA. Consequently, this work evaluates the reproducibility as the total variance of measurements without distinguishing the effects of individual factors. This reproducibility aligns with the VIM definition [52], as the variance estimation is conducted under varying conditions, including the number of images, the position of the component with respect to the markers and the camera location. Furthermore, in the case of the cobot, the time required to construct a sufficient set of images is considerably longer due to its size. Therefore, five measurement subsets are considered, containing 80, 85, 90, 95, and 100 images, respectively, each captured from various camera positions. Since the number of images is different, this change condition can account for the reproducibility.

Table 8 contains a summary of uncertainties, including the computation of the expanded uncertainty and the percentage relative uncertainty. Specifically, it can be noticed that contributions from resolution and numerical algorithms for dimensional evaluation, i.e., RANSAC, can be considered negligible. Also, thanks to the calibration of internal and external camera parameters, photogrammetry is highly accurate, thus making negligible the bias uncertainty contribution; the related variance is two order of magnitude smaller than the total variance. Thus, the overall uncertainty budget is dominated by the reproducibility. The considered methodology includes in the reproducibility some factors, namely the camera position and number of images, that are liable for systematic differences in the point cloud. These can be linked to qualitative effects related to coverage, quality of reconstruction, and interaction with the measurand surfaces; such effects cannot be corrected. Furthermore, their elimination is strongly task-based dependent and not always possible, e.g., large-scale mandate using multiple poses. Accordingly, propagating them provides a conservative uncertainty estimation by means of a practical methodology that allows ease of replication also for industrial practitioners. Traceability is established by relying on the measurement of reference artifacts calibrated, as detailed in Section 3.4 and depicted in Fig. 10, and propagating the uncertainty of the measured reference value and the bias related contribution [54, 57]. Specifically, the geometrical reference for the small-scale object is generated with the ATOS GOM ScanBox Series 4 [53]. In contrast, the reference geometry for the meso-scale is reconstructed using the API Laser Tracker and API iScan 3D laser line scanner [56]. Fig. 18 illustrates the best linear regression fit for the expanded uncertainty at each distance, also displaying the variation in percentage relative uncertainty

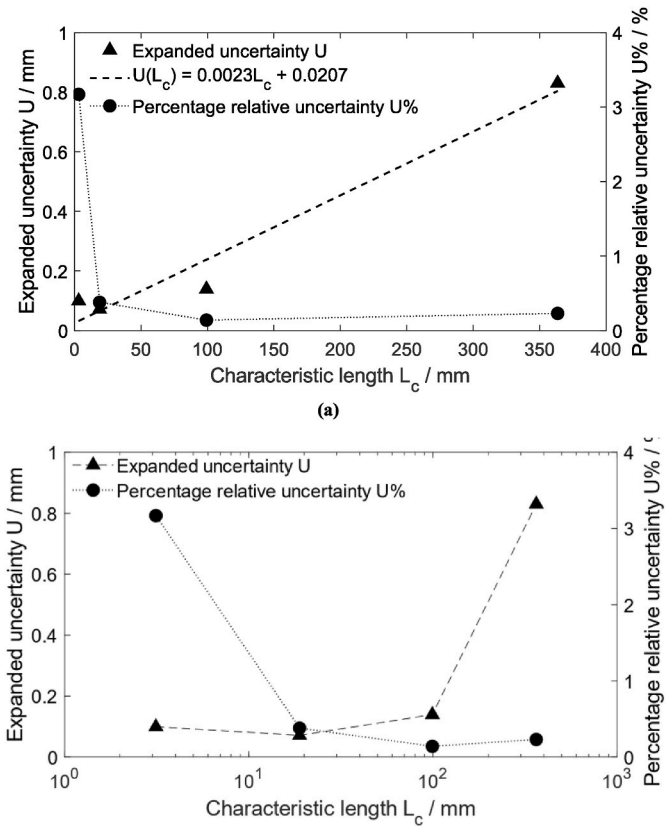

Fig. 18. Best linear regression fit for the expanded uncertainty at each characteristic length ($R^2 = 0.961$), and variation of percentage relative uncertainty; (a) linear scale, and (b) logarithmic scale.

across different distances. Thoroughly, Fig. 18a reports the linear scale, whereas the logarithmic plot can be observed in Fig. 18b.

By observing the results, the following comments can be made.

- The camera position affects the measurement, introducing a systematic factor, since it impacts the coverage and light interaction with the measurand surface.
- Despite the effect of camera position, the bias of geometrical characterization based on the average photogrammetric evaluation provides a negligible contribution to the measurement uncertainty, especially for small-scale objects.

Table 8
Summary of uncertainties and estimation of expanded uncertainty.

	D_{truss}		D_{sphere}		$D_{ballbar}$		D_{cobot}	
	Variance/mm^2	ν	Variance/mm^2	ν	Variance/mm^2	ν	Variance/mm^2	ν
Reproducibility	1.03E-03	23	6.18E-04	23	2.35E-03	23	8.04E-02	4
RANSAC Systematic	1.00E-20	100	1.00E-20	100	1.00E-20	100	1.00E-20	100
RANSAC Random	1.00E-04	100	1.00E-04	100	1.00E-04	100	1.00E-04	100
Bias	4.10E-04	23	1.12E-06	23	1.90E-03	23	6.21E-02	4
Reference[a]	7.47E-04	31	3.36E-04	8	2.82E-04	7	1.44E-03	10
Resolution	2.08E-04	100	2.08E-04	100	2.08E-04	100	5.33E-04	100
u^2/mm^2	2.49E-03		1.26E-03		4.84E-03		1.45E-01	
u/mm	4.99E-02		3.55E-02		6.92E-02		3.80E-01	
ν_y	86		51		57		8	
K	1.99		2.01		2.00		2.31	
U/mm	9.93E-02		7.13E-02		1.39E-01		8.77E-01	
$\overline{L_c}$/mm	3.13		18.86		99.26		363.52	
u%	1.60 %		0.19 %		0.07 %		0.10 %	
U%	3.17 %		0.38 %		0.14 %		0.24 %	

[a] Reference artifact contributions from Table 3 [59].

- Multiple camera positions are often required to manage meso- and large-scale geometrical complexity.
- Measurement reproducibility, possibly including multiple camera positions, dominates the uncertainty budget of dimensional characterization based on photogrammetry measurements.
- Excluding the truss, the relative measurement uncertainty exhibits a nearly constant pattern. The high expanded uncertainty observed for the truss highlights the criticality of measurement at very small measurand scales.
- The expanded uncertainty estimated across the different characteristic lengths exhibits a linear tendency, demonstrating a good agreement with the literature findings.

5. Conclusions

This work presented a combined qualitative and quantitative methodology for evaluating the performance of photogrammetry across different scales from 1 mm to 1 m. The qualitative analysis compared the scales by employing a set of sub-criteria that identified performance levels aligning with a five-level ordinal scale. The quantitative evaluation is carried out by identifying the sources of uncertainty and thus expanding them to fulfill a robust estimation of the expanded uncertainty.

The comparative qualitative analysis of photogrammetry across different scales reveals nuanced insights into its performance, remarkably when evaluated against criteria such as simplicity/time of use, measurement performance, and scale-dependent proficiency. Specifically.

- For the simplicity/time of use criterion, findings indicate that photogrammetry at the small-scale exhibits predominantly Medium/High (M/H) performance.
- The meso-scale performance falls within the Medium (M) range, suggesting that small-scale photogrammetry applications are notably more user-friendly and efficient than meso-scale applications.
- In terms of measurement performance, the analysis does not highlight a clear superiority of one scale over another. However, when evaluating scale-dependent proficiency, the meso-scale demonstrates higher performance.
- Consequently, while small-scale photogrammetry may offer benefits in terms of ease of use, meso-scale photogrammetry holds its advantages, particularly in contexts requiring specialized scale-dependent capabilities.
- The expected performance for larger scales of interest, specifically large-scale structures, is projected to be enhanced in terms of scale-dependent proficiency. The benefits derived from employing visual techniques for measurement and inspection underscore the utility of photogrammetry as a highly effective technique.

Additionally, this work provided a quantitative metrological benchmark of photogrammetry performance across multiple scales. Main results have highlighted that.

- Camera positioning introduces a systematic factor, which in setup for meso- and large-scale applications requiring multiple camera poses leads the reproducibility to be the primary contributor to the uncertainty budget.
- The relative measurement uncertainty decreases with an increase in the measurement scale, underscoring the applicability of photogrammetry in precision engineering applications.
- Furthermore, a discernible linear trend in expanded uncertainty across different scales states the consistency and potential accuracy of photogrammetry in dimensional analysis.

This paper significantly extends the application of photogrammetry within the field of precision engineering, industrial metrology, and quality control applications. By delving into the measurement accuracy, bias, and uncertainty within photogrammetric evaluations, the research provides a framework that enhances the reliability and precision of photogrammetry as a critical tool in these fields. Future research efforts will be directed toward integrating cameras with unmanned aerial vehicles (UAVs) for precision and quality engineering applications to measure and inspect large-volume structures considering an extension of the scales of interest beyond the limits addressed in this paper. A particular emphasis will be placed on the development of AI-Based methods for identifying surface defects and damage detection.

CRediT authorship contribution statement

Mattia Trombini: Writing – review & editing, Writing – original draft, Methodology, Data curation, Conceptualization. **Giacomo Maculotti:** Writing – review & editing, Formal analysis, Data curation. **Domenico Augusto Maisano:** Supervision, Project administration, Conceptualization. **Alfonso Pagani:** Writing – review & editing, Data curation, Conceptualization. **Fiorenzo Franceschini:** Writing – review & editing, Supervision, Methodology, Conceptualization.

Declaration of competing interest

The authors declare that they have no known competing financial interests or personal relationships that could have appeared to influence the work reported in this paper.

Aknowledgements

This study was carried out within the Space It Up project funded by the Italian Space Agency, ASI, and the Ministry of University and Research, MUR, under contract n. 2024-5-E.0 - CUP n. I53D24000060005.

Appendix A

A.1 Simplicity/time of use

Portability:	L: The equipment is very bulky and heavy, rendering it impractical for transportation and relegating its use to stationary or semi-stationary installations.
	L/M: The equipment is bulky and heavy, requiring considerable effort to move and may only be suitable for some locations.
	M: The equipment has an average weight and size, making it manageable to transport with some effort and planning.
	M/H: The equipment is relatively easy to transport but may require some effort or additional resources for specific locations.
	H: The lightweight and compact equipment allows easy transportation to any location without significant effort.
Accessory tools:	L: The component's size and fixed placement negate the use of accessory tools.
	L/M: Some difficulties with the component's manageability; accessory tools offer limited improvement.
	M: The component handling is manageable with minor inconveniences; accessory tools are moderately effective.

(*continued on next page*)

(*continued*)

	M/H: The component is maneuverable well; accessory tools improve photogrammetric efficiency with slight limitations.
	H: The component is easily maneuvered; accessory tools significantly enhance the photogrammetric process without restrictions.
Number of markers:	L: A significantly high quantity of markers is necessitated, which complicates management and may affect the workflow due to the object's size.
	L/M: A high quantity of markers is required, influenced by the object's dimensions, though it remains manageable with careful planning.
	M: A moderate quantity of markers is needed, reflecting a balance between the object's size and the ease of data management.
	M/H: The number of markers is not streamlined; however, the object's size has a minimal impact on the efficiency of the process.
	H: The smallest practical quantity of markers is employed, optimizing the process in relation to the object's size and facilitating straightforward data management.
Marker placement:	L: Marker placement is highly challenging, significantly impacting the measurement process.
	L/M: Marker placement is challenging, with some impact on measurement efficiency.
	M: Marker placement has a moderate difficulty level with a manageable impact on efficiency.
	M/H: Marker placement is relatively easy and has a minor impact on efficiency.
	H: Marker placement is straightforward, not impacting the measurement efficiency.
Set-up time:	L: Set-up is very time-consuming, significantly affecting productivity.
	L/M: Set-up takes longer than ideal, negatively impacting productivity.
	M: Set-up takes moderate time with a manageable impact.
	M/H: Set-up is reasonably quick, with minimal impact on productivity.
	H: Set-up is rapid, enhancing overall productivity.
Operator dexterity:	L: This level necessitates an elevated degree of proficiency and expertise from the operator, rendering the task challenging without specialized training.
	L/M: At this level, operators are required to demonstrate a heightened level of skill, which may present challenges without a certain degree of training.
	M: This classification calls for a moderate skill level attainable by operators possessing some degree of experience.
	M/H: This level requires a certain skill level but remains manageable for most operators with basic training.
	H: At this performance level, minimal skill acquisition is needed, rendering the task highly accessible for most operators.
Number of images:	L: The process necessitates a significantly high number of images, thereby greatly enhancing the complexity.
	L/M: The acquisition demands a large number of images, leading to extended processing duration.
	M: A moderate quantity of images is required, balancing manageability in both complexity and processing time.
	M/H: The operation calls for a slight number of images, yet this does not markedly impact processing efficiency.
	H: The minimal number of images needed ensures a highly efficient processing workflow.
Time for acquisition:	L: The acquisition process is prolonged, severely detracting from productivity.
	L/M: The acquisition duration is long, with a noticeable negative effect on productivity.
	M: The acquisition time is adequate, with manageable effects on productivity.
	M/H: The acquisition process is relatively swift, slightly enhancing productivity.
	H: The acquisition is expedited, significantly improving productivity.
Processing time:	L: Processing is very time-consuming, creating a significant bottleneck.
	L/M: Processing is time-consuming, affecting turnaround time.
	M: Processing takes a moderate amount of time, with a manageable impact on project timelines.
	M/H: Processing is reasonably quick, with minimal impact on timelines.
	H: Processing is rapid, greatly enhancing project throughput.
Post-processing heaviness:	L: Post-processing is extremely heavy due to significant noise reduction efforts.
	L/M: Post-processing is heavy, with a considerable focus on noise reduction.
	M: Moderate post-processing efforts required for noise reduction.
	M/H: Lighter post-processing with minimal noise reduction efforts needed.
	H: Minimal post-processing is required, with noise reduction being trivial.

A.2 Measurement performance

Information content:	L: Poor geometry reconstruction and color inconsistency; semantic information is largely absent.
	L/M: Below-average geometry reconstruction and color consistency; some semantic information is missing.
	M: Average geometry reconstruction and color consistency; some semantic information may be present.
	M/H: Above-average geometry reconstruction and color consistency; most semantic information is present.
	H: Excellent geometry reconstruction and color consistency; all semantic information is present.
Reconstruction quality:	L: The point cloud's quality and density are significantly compromised, leading to poor reconstruction results.
	L/M: The quality of reconstruction is suboptimal.
	M: The reconstruction is adequate. Complex parts still produce issues in the reconstruction's quality and density.
	M/H: The complexity is well-managed, and improvements in cloud density can be made.
	H: Exceptional quality and density of the point cloud are attained, ensuring superior reconstruction results.
Statistical investigation:	L: The statistical investigation becomes extremely time-consuming and impractical, hampered by the high number of images and the extended duration needed for uncertainty assessment.
	L/M: The statistical investigation process is notably time-intensive, necessitated by an increased number of images, which extends the time for uncertainty assessment.
	M: A balanced approach to statistical investigation, requiring a moderate number of images, balances time efficiency with thorough uncertainty assessment.
	M/H: Statistical investigation is reasonably efficient, facilitated by a manageable number of images, allowing for a more streamlined uncertainty assessment.
	H: The statistical investigation process is highly efficient, minimized in both the number of images required and the rapid completion of uncertainty assessment.
Noise:	L: The environmental noise significantly impacts the reconstruction due to the object's small proportion in the captured scene, overshadowed by the surroundings.
	L/M: The reconstructed cloud faces substantial environmental noise, as the object occupies a smaller area within the frame, reducing clarity.

(*continued on next page*)

(*continued*)

	M: The impact of environmental noise is moderate, with the object and surroundings balanced in a way that neither overwhelms the other.
	M/H: Environmental noise is less of a concern, with the object's presence in the frame sufficiently large to mitigate its effect.
	H: The object's substantial dominance in the frame minimizes environmental noise, enhancing the clarity and focus of the analysis.
Detection of small geometrical variation:	L: Inability to detect small geometrical variations due to the high uncertainty threshold of measurement instruments.
	L/M: Difficulty in detecting small geometrical variations with some limitations due to measurement uncertainty.
	M: Moderate capability in detecting geometrical variations with an acceptable uncertainty threshold.
	M/H: Reliable detection of small geometrical variations with low measurement uncertainty.
	H: Excellent detection of small geometrical variations with minimal measurement uncertainty.

A.3 Scale-dependent proficiency

Skill improvement:	L: Skill enhancement is minimal; operations are basic and do not benefit significantly from advanced technical or scientific skills.
	L/M: Some improvement in skill can optimize the process, which remains primarily straightforward with routine operations.
	M: Moderate skill development contributes to efficiency; the complexity of tasks is balanced with operational simplicity.
	M/H: Improved skills lead to notable gains in efficiency; technical tasks like camera positioning and exposure settings start to impact processing time.
	H: Advanced skill mastery greatly enhances operational efficiency; expertise in technical settings and equipment handling is crucial for process optimization.
Effective applicability:	L: Photogrammetry is generally unsuitable; the required precision and accuracy are beyond the method's capability, rendering it inefficient.
	L/M: Limited suitability of photogrammetry; it can be used with some success but may not meet all the requirements for precision and detailed analysis.
	M: Photogrammetry is moderately suitable; it provides a balance between ease of use and the level of detail required, though it may not fully meet high precision demands.
	M/H: Photogrammetry is quite suitable; it meets most of the objectives for measurement, offering a high level of detail, though with some limitations in precision.
	H: Photogrammetry is highly suitable; it effectively meets the specific context and objectives of the measurement, achieving the necessary precision and accuracy for comprehensive analysis.

References

[1] Pollock L, Abdelwahab AK, Murray J, Wild G. The need for aerospace structural health monitoring: a review of aircraft fatigue accidents. Int J Prognostics Health Manag 2021;12(3):1–16. https://doi.org/10.36001/ijphm.2021.v12i3.2368.

[2] Knapp S, Franses PH. Comprehensive review of the maritime safety Regimes: present status and recommendations for improvements. Transport Rev 2010;30(2): 241–70. https://doi.org/10.1080/01441640902985934.

[3] Campbell LE, Connor RJ, Whitehead JM, Washer GA. Benchmark for evaluating performance in visual inspection of fatigue cracking in steel bridges. J Bridge Eng 2020;25(1):04019128. https://doi.org/10.1061/(ASCE)BE.1943-5592.0001507.

[4] Bond LJ. Fundamentals of ultrasonic inspection. ASM International 2018;17: 155–68. https://doi.org/10.31399/asm.hb.v17.a0006470.

[5] Swornowski PJ. Scanning of the internal structure part with laser ultrasonic in aviation industry. Scanning 2011;33(5):378–85. https://doi.org/10.1002/sca.20260.

[6] Błachnio J, Chalimoniuk M, Kułaszka A, Borowczyk H, Zasada D. Exemplification of detecting gas turbine blade structure defects using the X-ray computed tomography method. Aerospace 2021;8(4):119. https://doi.org/10.3390/aerospace8040119.

[7] William LD, Abdelfatah MY. Corrosion detection in aircraft by X-ray backscatter methods. Appl Radiat Isot 2000;53(4):625–32. https://doi.org/10.1016/S0969-8043(00)00240-2.

[8] Agdas D, Rice JA, Martinez JR, Lasa IR. Comparison of visual inspection and structural-health monitoring as bridge condition assessment methods. J Perform Constr Facil 2016;30(3):04015049. https://doi.org/10.1061/(ASCE)CF.1943-5509.0000802.

[9] Garnier C, Pastor M-L, Eyma F, Lorrain B. The detection of aeronautical defects in situ on composite structures using Non Destructive Testing. Compos Struct 2011;93 (5):1328–36. https://doi.org/10.1016/j.compstruct.2010.10.017.

[10] Katunin A, Dragan K, Dziendzikowski M. Damage identification in aircraft composite structures: a case study using various non-destructive testing techniques. Compos Struct 2015;127:1–9. https://doi.org/10.1016/j.compstruct.2015.02.080.

[11] Golnabi H, Asadpour A. Design and application of industrial machine vision systems. Robot Comput Integrated Manuf 2007;23(6):630–7. https://doi.org/10.1016/j.rcim.2007.02.005.

[12] Wolfschläger D, Woltersmann J-H, Montavon B, Schmitt RH. Sheared edge defect segmentation using a convolutional U-Net for quantified quality assessment of fine blanked workpieces. Precis Eng 2022;75:129–41. https://doi.org/10.1016/j.precisioneng.2022.01.010.

[13] Leizea I, Herrera I, Puerto P. Calibration procedure of a multi-camera system: process uncertainty budget. Sensors 2023;23(2):589. https://doi.org/10.3390/s23020589.

[14] Puerto P, Leizea I, Herrera I, Barrios A. Analyses of key variables to industrialize a multi-camera system to guide robotic arms. Robotics 2023;12(1):10. https://doi.org/10.3390/robotics12010010.

[15] Kholkhujaev J, Maculotti G, Genta G, Galetto M, Inoyatkhodjaev J. Non-contact articulated robot-integrated gap and flushness measurement system for automobile assembly. IEEE Access 2022;10:86528–41. https://doi.org/10.1109/ACCESS.2022.3199066.

[16] Franceschini F, Galetto M, Maisano D, Mastrogiacomo L. Combining multiple Large Volume Metrology systems: competitive versus cooperative data fusion. Precis Eng 2016;43:514–24. https://doi.org/10.1016/j.precisioneng.2015.09.014.

[17] Weckenmann A, Jiang X, Sommer K-D, Neuschaefer-Rube U, Seewig J, Shaw L, Estler T. Multisensor data fusion in dimensional metrology. CIRP Annals 2009;58 (2):701–21. https://doi.org/10.1016/j.cirp.2009.09.008.

[18] Zhou HF, Dou HY, Qin LZ, Chen Y, Ni YQ, Ko JM. A review of full-scale structural testing of wind turbine blades. Renew Sustain Energy Rev 2014;33:177–87. https://doi.org/10.1016/j.rser.2014.01.087.

[19] Baqersad J, Poozesh P, Niezrecki C, Avitabile P. Photogrammetry and optical methods in structural dynamics – a review. Mech Syst Signal Process 2017;86: 17–34. https://doi.org/10.1016/j.ymssp.2016.02.011.

[20] Roca D, Lagüela S, Díaz-Vilariño L, Armesto J, Arias P. Low-cost aerial unit for outdoor inspection of building façades. Autom ConStruct 2013;36:128–35. https://doi.org/10.1016/j.autcon.2013.08.020.

[21] Zhang D, Watson R, Dobie G, MacLeod C, Khan A, Pierce G. Quantifying impacts on remote photogrammetric inspection using unmanned aerial vehicles. Eng Struct 2020;209:109940. https://doi.org/10.1016/j.engstruct.2019.109940.

[22] Estler WT, Edmundson KL, Peggs GN, Parker DH. Large-scale metrology – an update. CIRP Annals 2002;51(2):587–609. https://doi.org/10.1016/S0007-8506(07)61702-8.

[23] Franceschini F, Galetto M, Maisano D, Mastrogiacomo L, Pralio B. Distributed large-scale dimensional metrology: new insights. Springer Science & Business Media; 2011.

[24] Maisano DA, Mastrogiacomo L, Franceschini F, Capizzi S, Pischedda G, Laurenza D, Gomiero G, Manca G. Dimensional measurements in the shipbuilding industry: on-site comparison of a state-of-the-art laser tracker, total station and laser scanner. J Inst Eng Prod 2023;17(3):625–42. https://doi.org/10.1007/s11740-022-01170-7.

[25] Feng D, Feng MQ. Computer vision for SHM of civil infrastructure: from dynamic response measurement to damage detection – a review. Eng Struct 2018;156: 105–17. https://doi.org/10.1016/j.engstruct.2017.11.018.

[26] Zhao S, Kang F, Li J, Ma C. Structural health monitoring and inspection of dams based on UAV photogrammetry with image 3D reconstruction. Autom ConStruct 2021;130:103832. https://doi.org/10.1016/j.autcon.2021.103832.

[27] de Pastre M-A, Toguem Tagne S-C, Anwer N. Test artefacts for additive manufacturing: a design methodology review. CIRP Journal of Manufacturing Science and Technology 2020;31:14–24. https://doi.org/10.1016/j.cirpj.2020.09.008.

[28] Catalucci S, Senin N, Sims-Waterhouse D, Ziegelmeier S, Piano S, Leach R. Measurement of complex freeform additively manufactured parts by structured light and photogrammetry. Measurement 2020;164:108081. https://doi.org/10.1016/j.measurement.2020.108081.

[29] Schmitt RH, Peterek M, Morse E, Knapp W, Galetto M, Härtig F, Goch G, Hughes B, Forbes A, Estler WT. Advances in large-scale metrology – review and future trends. CIRP Annals 2016;65(2):643–65. https://doi.org/10.1016/j.cirp.2016.05.002.

[30] Franceschini F, Galetto M, Genta G. Multivariate control charts for monitoring internal camera parameters in digital photogrammetry for LSDM (Large-Scale Dimensional Metrology) applications. Precis Eng 2015;42:133–42. https://doi.org/10.1016/j.precisioneng.2015.04.008.

[31] Savio E, De Chiffre L, Schmitt R. Metrology of freeform shaped parts. CIRP Annals 2007;56(2):810–35. https://doi.org/10.1016/j.cirp.2007.10.008.

[32] Liu S, Zhang M, Kadam P, Kuo C. 3D Point cloud analysis. Springer; 2021.
[33] Mirzaei K, Arashpour M, Asadi E, Masoumi H, Bai Y, Behnood A. 3D point cloud data processing with machine learning for construction and infrastructure applications: a comprehensive review. Adv Eng Inf 2022;51:101501. https://doi.org/10.1016/j.aei.2021.101501.
[34] Wang Q, Tan Y, Mei Z. Computational methods of acquisition and processing of 3D point cloud data for construction applications. Arch Comput Methods Eng 2020;27:479–99. https://doi.org/10.1007/s11831-019-09320-4.
[35] El Ghazouali S, Vissiere A, Lafon L-F, Bouazizi M-L, Nouira H. Optimised calibration of machine vision system for close range photogrammetry based on machine learning. Journal of King Saud University - Computer and Information Sciences 2022;34(9):7406–18. https://doi.org/10.1016/j.jksuci.2022.06.011.
[36] Ioli F, Pinto A, Pinto L. Uav photogrammetry for metric evaluation of concrete bridge cracks. Int Arch Photogram Rem Sens Spatial Inf Sci 2022:1025–32. https://doi.org/10.5194/isprs-archives-XLIII-B2-2022-1025-2022. XLIII-B2-2022.
[37] Benzon H-H, Chen X, Belcher L, Castro O, Branner K, Smit J. An operational image-based digital twin for large-scale structures. Appl Sci 2022;12(7):3216. https://doi.org/10.3390/app12073216.
[38] Zhang H, Eastwood J, Isa M, Sims-Waterhouse D, Leach R, Piano S. Optimisation of camera positions for optical coordinate measurement based on visible point analysis. Precis Eng 2021;67:178–88. https://doi.org/10.1016/j.precisioneng.2020.09.016.
[39] Isa MA, Sims-Waterhouse D, Piano S, Leach R. Volumetric error modelling of a stereo vision system for error correction in photogrammetric three-dimensional coordinate metrology. Precis Eng 2020;64:188–99. https://doi.org/10.1016/j.precisioneng.2020.04.010.
[40] Mikhail EM, Bethel JS, McGlone JC. Introduction to modern photogrammetry. John Wiley & Sons; 2001.
[41] Luhmann T, Robson S, Kyle S, Harley I. Close range photogrammetry. Caithness, UK: Wiley Whittles Publishing; 2006.
[42] Zhang S, Cheng S, Jin Z. Visual measurement method and application of mobile manipulator pose estimation based on PPMCC-IMM filtering. IEEE Trans Instrum Meas 2023;72:1–12. https://doi.org/10.1109/TIM.2023.3268468.
[43] Basler product documentation. acA2500-14uc, https://docs.baslerweb.com/aca2500-14uc. [Accessed 25 January 2024].
[44] Basler Product Documentation. Basler lens C125-0818-5M-P. https://docs.baslerweb.com/c125-0818-5m. [Accessed 25 January 2024].
[45] Agisoft. Discover intelligent photogrammetry with Metashape. https://www.agisoft.com/. [Accessed 31 January 2024].
[46] Galetto M, Verna E, Genta G. Effect of process parameters on parts quality and process efficiency of fused deposition modeling. Comput Ind Eng 2021;156:107238. https://doi.org/10.1016/j.cie.2021.107238.
[47] Apium. Apium P220. https://apiumtec.com/en/industrial-3d-printer. [Accessed 10 January 2024].
[48] Universal Robots: Collaborative robotic automation. Cobots from universal robots. https://www.universal-robots.com/. [Accessed 12 February 2024].
[49] Gervasi R, Mastrogiacomo L, Maisano DA, Antonelli D, Franceschini F. A structured methodology to support human–robot collaboration configuration choice. J Inst Eng Prod 2022;16:435–51. https://doi.org/10.1007/s11740-021-01088-6.
[50] Gervasi R, Mastrogiacomo L, Franceschini F. A conceptual framework to evaluate human-robot collaboration. Int J Adv Des Manuf Technol 2020;108:841–65. https://doi.org/10.1007/s00170-020-05363-1.
[51] Fisher RA. Design of experiments. Edinburgh: Oliver and Boyd; 1935.
[52] JCGM 100. Evaluation of measurement data — guide to the expression of uncertainty in measurement (GUM). first ed. Sèvres; 2008.
[53] GOM Metrology. ATOS ScanBox Series 4. https://www.gom.com/en/products/3d-measuring-machines/atos-scanbox-series-4. [Accessed 22 January 2024].
[54] ISO 10360-13:2021 Geometrical product specifications (GPS). Acceptance and reverification tests for coordinate measuring systems (CMS) - Part 13: optical 3D CMS. 2021. Geneva.
[55] Jaganmohan P, Muralikrishnan B, Lee V, Ren W, Icasio-Hernández O, Morse E. VDI/VDE 2634–1 performance evaluation tests and systematic errors in passive stereo vision systems. Precis Eng 2023;79:310–22. https://doi.org/10.1016/j.precisioneng.2022.11.005.
[56] API. API iSCAN3D. https://apimetrology.com/iscan3d/. [Accessed 31 January 2024].
[57] ISO 10360-10:2021 Geometrical product specifications (GPS). Acceptance and reverification tests for coordinate measuring systems (CMS) - Part 10: laser Trackers. 2021. Geneva.
[58] ISO 14253-2:2011 Geometrical product specifications (GPS). Inspection by measurement of workpieces and measuring equipment - Part 2: guidance for the estimation of uncertainty in GPS measurement. In: Calibration of measuring equipment and in product verification; 2011. Geneva.
[59] Gayton G, Isa M, Su R, Leach R. Evaluating and propagating uncertainty in digital fringe projection systems. In: Optical measurement systems for industrial inspection XII, vol. 11782. SPIE; 2021. p. 302–16. https://doi.org/10.1117/12.2592426.
[60] Sankowski W, Włodarczyk M, Kacperski D, Grabowski K. Estimation of measurement uncertainty in stereo vision system. Image Vis Comput 2017;61:70–81. https://doi.org/10.1016/j.imavis.2017.02.005.
[61] Fei L, Dantan J-Y, Baudouin C, Du S. Calibration and uncertainty estimation of non-contact coordinate measurement systems based on Kriging models. Precis Eng 2019;57:16–29. https://doi.org/10.1016/j.precisioneng.2019.02.004.
[62] Galetto M, Genta G, Maculotti G. Single-step calibration method for nano indentation testing machines. CIRP Annals 2020;69(1):429–32. https://doi.org/10.1016/j.cirp.2020.03.015.
[63] Maculotti G, Genta G, Galetto M. An uncertainty-based quality evaluation tool for nanoindentation systems. Measurement 2024;225:113974. https://doi.org/10.1016/j.measurement.2023.113974.
[64] JCGM 200. International vocabulary of metrology – basic and general concepts and associated terms (VIM). third ed. Sèvres; 2012.
[65] Maculotti G, Ulrich L, Olivetti EC, Genta G, Marcolin F, Vezzetti E, Galetto M. A methodology for task-specific metrological characterization of low-cost 3D camera for face analysis. Measurement 2022;200:111643. https://doi.org/10.1016/j.measurement.2022.111643.
[66] Fischler MA, Bolles RC. Random sample consensus: a paradigm for model fitting with applications to image analysis and automated cartography. Commun ACM 1981;24(6):381–95. https://doi.org/10.1145/358669.358692.
[67] Morelli L, Karami A, Menna F, Remondino F. Orientation of images with low contrast textures and transparent objects. Int Arch Photogram Rem Sens Spatial Inf Sci 2022:77–84. https://doi.org/10.5194/isprs-archives-XLVIII-2-W2-2022-77-2022. XLVIII-2/W2-2022.
[68] Motayyeb S, Fakhri SA, Varshosaz M, Pirasteh S. Enhancing contrast of images to improve geometric accuracy of a uav photogrammetry project. Int Arch Photogram Rem Sens Spatial Inf Sci 2022;43:389–98. https://doi.org/10.5194/isprs-archives-XLIII-B1-2022-389-2022.
[69] Trombini M, Maisano DA, Pagani A. Photogrammetric analysis for inspection and damage detection: preliminary assessment and future extension to large-volume structures. Aerospace Science and Engineering: III Aerospace PhD-Days 2023;33:355–61. https://doi.org/10.21741/9781644902677-52.
[70] Gibbons JD, Chakraborti S. Nonparametric statistical inference: revised and expanded. CRC Press; 2014.
[71] Rupnik E, Daakir M, Marc PD. MicMac–a free, open-source solution for photogrammetry. Open geospatial data, software and standards 2017;2(1):1–9. https://doi.org/10.1186/s40965-017-0027-2.